Green Chemistry

CRITICAL REVIEW

View Article Online
View Journal | View Issue

Cite this: *Green Chem.*, 2026, **28**, 3936

Combining cellulose substrates and perovskites in sustainable solar cells is possible: a systematic literature review offering realistic solutions

Joaquín Valdez García, *[a] Mahboubeh Hadadian, [a] Vidushi Aggarwal, [a] Sirius Yli-Paavola, [a] Joice Kaschuk, [b] Riikka Suhonen, [c] Marja Välimäki [c] and Kati Miettunen *[a]

The aim of this article is to provide direction for the advancement of cellulose films as sustainable substrates for perovskite solar cells (PSCs). Cellulose, the most abundant biopolymer on Earth, represents a viable, renewable alternative to glass and synthetic polymers when subjected to appropriate modifications. It can be customized *via* crosslinking, plasticization, and functionalization to increase flexibility and solvent resistance while decreasing gas permeation, surface roughness, and thermal expansion. The adoption of cellulose can drive transformative changes in PSC processing, facilitating the integration of sustainable electrode materials and greener alternatives to toxic solvents, as well as the replacement of high-temperature treatments. Although the literature contains numerous solutions to specific challenges, these findings are scattered across different fields and must be critically assessed for PSC suitability. In this article, we critically review alternative fabrication methods and form a step-by-step multidisciplinary strategy to alter both cellulose and PSC fabrication protocols for the development of sustainable next-generation solar cells.

Received 6th October 2025,
Accepted 2nd January 2026

DOI: 10.1039/d5gc05281e

rsc.li/greenchem

Green foundation

1. Here we discussed the integration of cellulose substrates in perovskite solar cells, the improvement of cellulose films with some green additives, the replacement of perovskite solvents with greener options, and alternative fabrication methods to reduce solvent usage.
2. We believe the integration of cellulose substrates in perovskite solar cells can improve the recyclability of solar energy devices, as well as accelerate the production of cheaper solar cells *via* printing and other wet deposition methods.
3. The perovskite solar cell field needs to anticipate and adapt to future needs through improved designs that focus on recyclability and the inclusion of renewable materials. Similarly, the cellulose field will have to adapt to the needs of the optoelectronics industry. In our review, we delineate how these two fields could come together through a green chemistry approach to retain their sustainability.

Introduction

Solar energy harvesting technologies are crucial for procuring clean energy. To beat climate change and quench our need for electricity, vast quantities of solar panels need to be manufactured and deployed. Perovskite solar cells (PSCs) have emerged as alternatives to silicon thanks to their high-volume and cost-efficient production, their high efficiency, and low-levelized cost of energy.[1] Their environmental, social, and economic sustainability is taking center-stage as they enter the market, necessitating rigorous attention to both material selection and assembly processes.

The fabrication of PSCs involves depositing very thin layers (<1 μm) of materials with distinct optoelectronic functions onto a substrate that ranges from 50 μm to 2 mm in thickness. The substrate constitutes the bulk of the device, thereby playing a major role in the device's life-cycle environmental impact[2] as well as in the recovery of environmentally hazardous and economically valuable components.[3] Historically, a variety of materials have been employed as substrates in flexible solar cells, each with their own advantages and disadvantages (Table 1).

Glass is desirable because of its excellent optical transmittance, which allows the majority of incident light to enter the active layer; its chemical inertness regarding the solvents used

[a]*Department of Mechanical and Materials Engineering, Faculty of Technology, University of Turku, Vesilinnantie 5, Turku FI-20500, Finland. E-mail: jvagar@utu.fi, kati.miettunen@utu.fi*
[b]*Physical Chemistry and Soft Matter Group, Wageningen University & Research, Wageningen, the Netherlands*
[c]*VTT Technical Research Centre of Finland Ltd, Digital Technologies, Kaitoväylä 1, Oulu FI-90590, Finland*

Table 1 Comparison of the physical properties of various photovoltaic substrate materials

Property	Glass	Metal foil	PET or PEN	Cellulose
Transparency	✓	✗	✓	✓[a]
Flexibility	Flexible up to 100 μm	✓	✓	✓[a]
Resistance to solvents used in PSC fabrication	✓	✓	✓	✓[a]
Low surface roughness	✓	✗	✓	✓[a]
Oxygen blocking	✓	✓	✗	✗[a]
Water vapor blocking	✓	✓	✗	✓[a]
Low coefficient of thermal expansion (CTE)	✓	✓	✗	✓[a]
Recyclability in photovoltaics	✓	✓	✗	✓
Price	$$$	$$	$	$

[a] Requires modifications.

in PSC fabrication; its mechanical robustness; its ability to withstand high temperatures; and it has low oxygen and water vapor transmission rates (OTR and WVTR, respectively).[4] However, its main drawback is rigidity, which renders it unsuitable for high-volume roll-to-roll (R2R) printing techniques. While flexible glass (FG) has been utilized to fabricate solar cells, its adoption is hindered by its inherent brittleness,[5] high cost,[6] and the limited market for solar glass waste following recycling.[7,8]

Metal foils are inherently highly conductive, excellent at blocking oxygen and moisture, highly flexible, and have shown some potential in emerging solar cells.[9,10] Nonetheless, their opacity and high surface roughness represent major impediments.[5] Their opacity requires that the top contact be transparent and flexible, which limits the choice of top electrode materials.[11] Furthermore, their surface roughness is in the order of microns, which requires planarization (*i.e.*, polishing) or the use of passivation layers.[5] Synthetic polymers, such as polyethylene terephthalate (PET) and polyethylene naphthalate (PEN), are the preferred materials for R2R fabrication because of their high transparency and flexibility, low cost, and low weight. Despite their positive properties, synthetic polymer substrates are limited by thermal and solvent instability and require low oxygen and water vapor barrier layers to block gas and moisture.[5]

Major advancements have been made in using cellulose and its derivatives to produce films with traits desirable for solar cell substrates.[12,13] Cellulose materials can already reach transparency and surface roughness levels comparable to glass, and similar mechanical properties to those of synthetic polymers with an increased thermal stability.[14] Cellulose is a nontoxic, low-cost material and the most abundant biopolymer on the planet; it can be obtained from various renewable sources and side streams. The modification of cellulose for optoelectronics begins with achieving high transparency. When unmodified, in their macroscopic structure, cellulose fibers form long networks that form light-scattering pores, resulting in opaque, white materials like paper and cotton.[15] These materials can be transformed into transparent films through several strategies, including modification and defibrillation. The most consolidated and reliable approach is to produce cellulose derivatives, which involves replacing one or more of the three reactive hydroxyl groups (–OH) on the cellulose chain with a functional group (esters, ethers, *etc.*; see Fig. 1).[16,17] The degree of substitution (DS), which denotes the number of –OH groups substituted, can range from 0 to 3 and largely dictates the properties of the resulting material.[18]

Another critical aspect of cellulose is its solubility and interaction with solvents. The hierarchical and recalcitrant structure of unmodified cellulose originates from the semicrystalline structure and extensive intra- and intermolecular hydrogen bond network between chains, which prevents the dissolution of cellulose in most commonly used solvents (ethanol, acetone, *etc.*).[17] These molecular interactions are altered when cellulose is modified, resulting in cellulose derivatives that are soluble in common solvents, depending on the functional group and DS. Furthermore, the cellulose hydrophilicity and its amorphous regions facilitate strong water bonding and trapping, allowing unmodified cellulose materials to absorb larger quantities without being dissolved.[20] Notably, cellulose derivatives may exhibit divergent swelling behaviors because certain functional groups have high levels of hydrophobicity compared to those in unmodified cellulose.

In the cellulose field there is a concept known as the "cellulose gap". Cotton demand in textile production is very high; cotton production is not expected to meet this demand, as its production is very water intensive, and the textile industry is working on developing cellulose fibers that can complement cotton.[21] Conversely, cellulose sourced from bacteria is quite costly and is used in specialized applications like biomedicine.[22] Currently, wood is the biggest alternative to cotton due to low costs and large availability.[21] As such, most of the commercially available cellulose to make films, membranes, and hydrogels is sourced from wood. Unlike in fibers, nanofibers,[23] and nanocrystals,[24] after derivatizing and functionalizing polymeric cellulose and cellulose nanocrystals for transparent films in optoelectronic applications, its source has little impact other than the degree of polymerization (DP). At this point, its functional groups, its DS, and whether or not it has been crosslinked or plasticized have a much greater impact on its properties.

From a processability standpoint, unmodified cellulose cannot be processed in a manner similar to synthetic polymers due to its high glass transition temperatures: the amount of thermal energy required to break the intermolecular hydrogen bonds of unmodified cellulose is so high that cellulose degrades before melting.[18] One of the strategies used to produce cellulose substrates involves the dissolution and regeneration (solvent removal) of films.[25] The properties of these films depend on a variety of factors, ranging from their new functional groups, their DS and size of the chain, their drying conditions, the surface on which they were cast, and

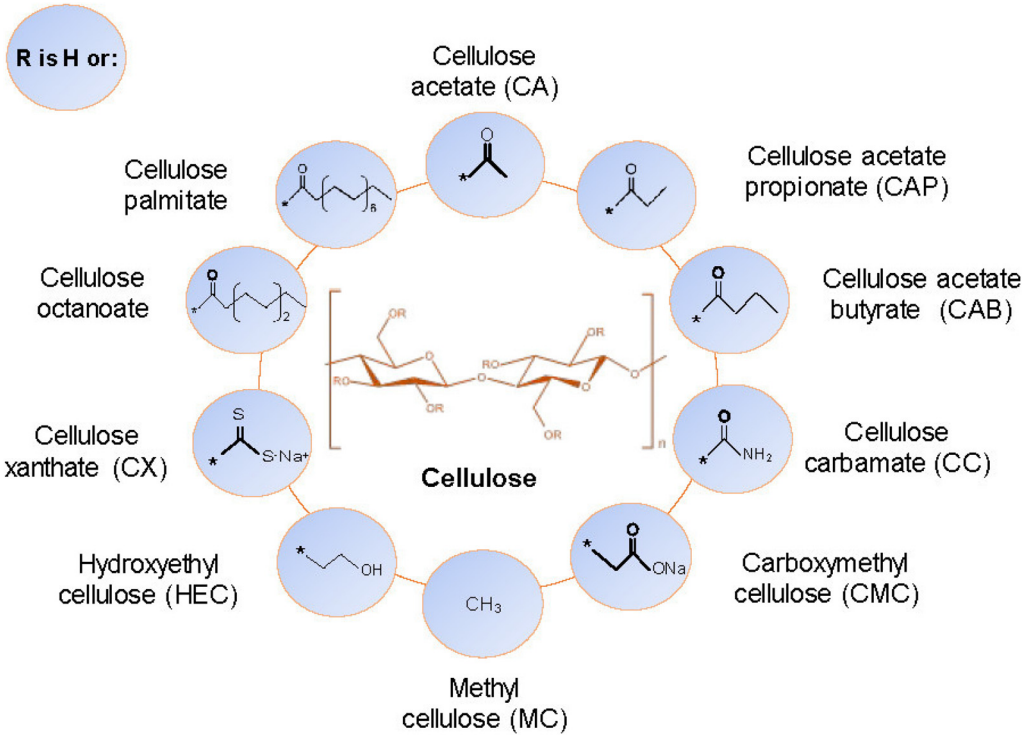

Fig. 1 Chemical structure of various cellulose derivatives. R can be a hydrogen or one of the groups around the cellulose molecule, reproduced from ref. 19 with permission from the American Chemical Society,19 Copyright 2022.

their porosity, among others. Controlling these parameters is key to making viable cellulose substrates for solar cells.

Two properties stand out when comparing cellulose films to currently used synthetic polymers: their solvent resistance and low thermal expansion. During fabrication, solar cell layers expand and contract along with the substrate, which leads to cracks that can reduce device performance and stability. Cellulose has a very low coefficient of thermal expansion (CTE) (0.1–158 ppm K^{-1} (ref. 26 and 27)) compared with synthetic polymers (12–122 ppm K^{-1} (ref. 28–30)), resulting in a more consistent PSC fabrication. Furthermore, some cellulose derivatives exhibit strong resistance to many solvents commonly used in PSC fabrication (see section Solvent resistance), while others can be crosslinked to obtain similar durability.[31]

A seldom-discussed advantage of cellulose is that it facilitates the recycling of solar cells. Glass and encapsulant resins are among the biggest hindrances associated with solar panel recycling, because they complicate separating valuable materials such as silver and high-quality silicon from shredded solar panel waste.[32] Glass, PET, and PEN coated with a thin layer of indium tin oxide (ITO) are the most commonly used substrates in PSCs. ITO accounts for most of a PSC's carbon emissions due to the energy-intensive vacuum deposition process required.[33] It can be recovered from glass using a chemical bath,[8] but panel encapsulation makes this difficult.[34] In contrast to glass substrates, PET and PEN can be easily burned in pyrolysis processes to extract valuable metals.[3] However, aside from bioPET,[35] they are derived from fossil sources. Thin cellulose substrates further concentrate the value of solar cell materials, making recycling economically viable at the end of the product's lifespan.[3] Since solar cells are meant to be encapsulated to maximize stability and efficiency over time, cellulose is not expected to degrade since it is not in an environment with bacteria, soil, and moisture.[19] Therefore, the recycling route for solar cells made on renewable cellulose is to degrade it only at the end of the device lifetime to allow for material recovery, either by burning it or by degrading it through photochemical means.[19]

As polymers are the most popular substrate materials when making flexible devices, most research is focused on the same. Notably, cells with a power conversion efficiency (PCE) lower than 20% are made of $MAPbI_3$ perovskite, one of the first perovskite compositions used, and higher efficiencies are reached by using perovskites with more complicated stoichiometries and compositions. While there is still room for improvement, Li *et al.*'s work demonstrated that cellulose films are viable substrates for PSCs and can achieve 13.1% efficiency.[36] Nevertheless, physical vapor deposition techniques are costly to implement and require high initial investments; cellulose, being the quintessential printing material, calls for solution-based R2R-compatible deposition methods. Table 2 provides a summary of high-performing flexible PSCs.

The PSC fabrication process imposes many requirements on cellulose (see Table 1). Many strategies are available to achieve these properties, but these are typically found in fields very different from photovoltaics, such as food packaging,

Table 2 High-performance PSCs on flexible substrates

Substrate	Structure	PCE [%]	J_{SC} [mA cm^{-2}]	V_{OC} [V]	FF [%]	Active area [cm^2]	Ref.
FG	FG/ITO/SnO_2/m-TiO_2/$MAPbI_3$/Spiro-OMeTAD/Au	15.8	22.83	1.09	79.1	0.08	37
Titanium foil	Ti/TiO_2/$MAPbI_3$/PTAA/Graphene/PDMS	15.0	18.70	1.08	74.4	1	38
Steel foil	Stainless steel/ITO/NiO_x/MeO-2PACz/(CsFAMA) ($(CsPbI_3)_{0.13}(FAPbI_3)_{0.85}(MAPbBr_3)_{0.02}$)/DMI/$C_{60}$/BCP/Ag	20.70	23.30	1.11	80.15	1.012	39
PET	PET/ITO/CBD-SnO_2/$(RbFAMA)Pb(ICl)_3$/Spiro-OMeTAD/Au	25.65	25.90	1.19	83.39	1	40
PEN	PEN/ITO/SnO_2-DNS//$(CsFAMA)Pb(BrICl)_3$/Spiro-OMeTAD/Au	23.16	24.85	1.13	82.2	1	41
PI	PI/ITO/PF-doped SnO_2/$(CsFAMA)Pb(BrICl)_3$/Spiro-OMeTAD/Au	23.31	24.87	1.16	80.80	1	42
Cellulose	Cellophane/TiO_2/Ag/TiO_2/C_{60}/CPTA/$MAPbI_3$/Spiro-OMeTAD/Au	13.19	17.81	1.04	71.30	Unspecified, <1	36

drug delivery, and battery membrane technologies, which have varying requirements for cellulose films. Furthermore, their applicability requires a critical assessment. This article fills the existing gap in the literature by reviewing relevant and potential solutions. The aim of our analysis is to shed light on the modifications required for cellulose to work as a good substrate in PSCs and on ways to adapt PSC fabrication methods to cellulose films, addressing both cellulose and solar cell audiences. The article begins with an analysis of PSC substrate materials and fabrication processes currently used, followed by a strategy on how to modify both the cellulose films and the typical PSC processing routes. As the need for clean energy sources increases, the more our devices need to adapt to sustainable designs. Understanding how to adapt biobased alternatives becomes critical for the development of next-generation solar cells.

The process of making a solar cell

A PSC is a stack of functional layers (Fig. 2); what layers are included and how they are arranged depends on many factors. The first component to consider is the active layer, and its bandgap dictates which charge transport layers (CTLs) can be used and how they need to be modified to match their band levels. Accordingly, the deposition sequence depends on the CTL deposition methods. Since the perovskite layer is vulnerable to solvents and high temperatures, it is advisable to first deposit the CTL that requires solvents and temperatures incompatible with the perovskite. The PSC structure is defined by whether the electron transport layer (ETL) or the hole transport layer (HTL) is deposited first, namely NIP (or regular) or PIN (or inverted), respectively.[43]

PSC fabrication is generally done on glass or polymeric substrates covered with a transparent conductive oxide (TCO). The methods used greatly depend on the fabrication scale; spin coating on glass/fluorine-doped tin oxide (FTO) or glass/ITO is favored at a laboratory scale, while coating or printing on PET/ITO or PEN/ITO is more common in high-volume industrial fabrication. Nevertheless, the deposition steps for both are quite similar (Fig. 3). The first step is the TCO patterning, normally done through chemical etching or laser patterning, although this process may be skipped in certain situations.[44] Next, the substrate is washed in different solvents to remove any residues that could interfere with the first CTL deposition. The substrate is treated with UV-ozone (UV-O_3) or plasma to increase its wettability, and the first CTL is immediately deposited, typically followed by thermal annealing. The active layer is then deposited, followed by another annealing step to crystallize the perovskite. Once the substrates have cooled down enough, the next CTL is deposited, followed by the thermal evaporation of the top electrode.[45] Depending on the materials used and the associated process, some steps are carried out inside a nitrogen-filled glovebox to prevent oxygen and moisture from interfering with the layers. Current research is focused on adapting PSC production to less restrictive environments and moving away from expensive vacuum-based, energy-intensive fabrication methods and special

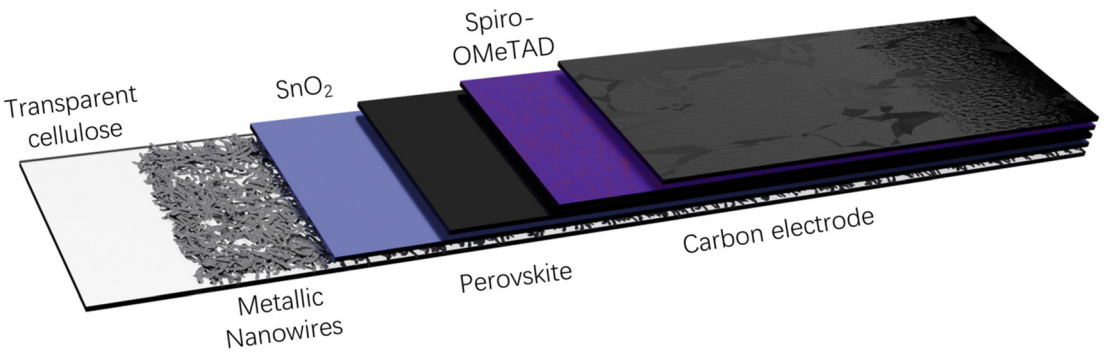

Fig. 2 Envisioned PSC (NIP architecture) made on a cellulose substrate.

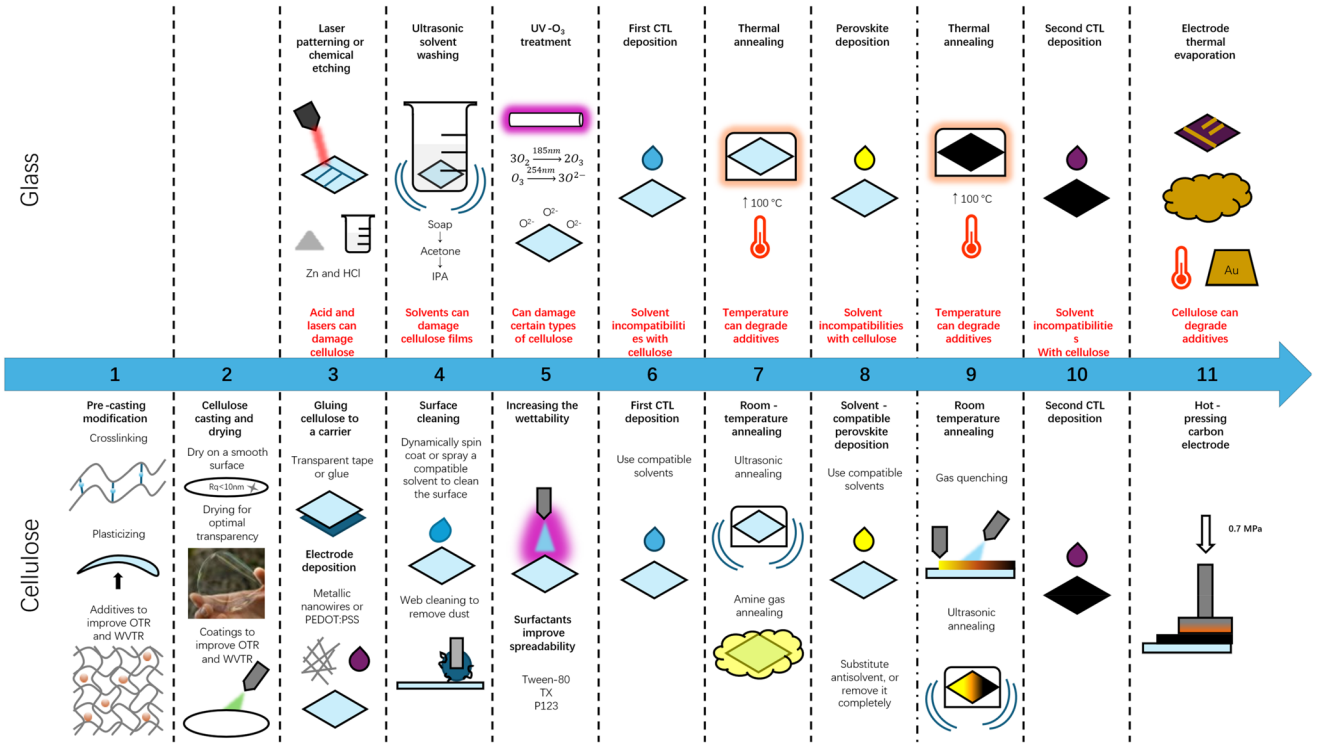

Fig. 3 Schematic of typical fabrication processes for PSCs on glass (upper panel) and the proposed or modified processes designed for compatibility with cellulose substrates (lower panel).

atmospheres, and toward wet deposition methods that are easier to implement.

The regular wet-method processing route presents many challenges when using unmodified cellulose films. First, the acid to etch ITO could damage cellulose. Many researchers have proposed the use of metallic nanowires instead, considering ITO's poor sustainability, but this approach requires prepatterning them, as they cannot be removed if embedded. Second, solvent washing can be problematic; some solvents may cause the cellulose fibers to redisperse or may infiltrate the film and cause it to swell. While UV-O_3 treatments break the carbon bonds in organic matter to volatilize contaminants on inorganic surfaces, this can damage cellulose films and make them more reactive, increasing solvent absorption. Third, additional plasticizers may be required to ensure that cellulose has sufficient flexibility during the PSC fabrication process. These plasticizers degrade at around 120 °C,[46] which limits the thermal steps in the process. Lastly, thermal annealing can decrease the mechanical properties of cellulose, making it more difficult to handle.[47]

Considering the above, we devised a PSC processing route on cellulose substrates based on strategies scattered across different fields to further advance the integration of biobased materials into next-generation solar cells (Fig. 3).

Step 1: preparing the cellulose suspensions and solutions

Before casting cellulose films, the cellulose solutions must be homogeneously produced and altered to provide cellulose with additional properties to endure PSC fabrication. The first thing to consider is the solvents used. Two options in this regard are (i) to employ a cellulose type compatible with the selected solvent or (ii) to crosslink the cellulose chains to avoid redispersion. Crosslinking can also decrease the film's thermal expansion. Next, cellulose can be mixed with plasticizers to increase the resulting film's mechanical strength and flexibility. Finally, different additives can be mixed in the cellulose matrix to give the resulting films gas-blocking properties for PSC protection.

Solvent resistance. The production of cellulose derivative films *via* dissolution and regeneration is an easier and greener process than the production of synthetic films such as PET and PEN. The disadvantage is that cellulose films may redisperse once in contact with different solvents (Fig. 4) or lose their mechanical properties if the atmosphere is saturated with solvent fumes. Therefore, the choice of cellulosic material is highly dependent on its resistance to the solvents used in the fabrication process.

Table 3 shows how commonly used solvents in solar cell fabrication affect cellulose films. The effect 15 different solvents have on cellulose films is judged by their visual appearance. After rubbing a solvent-soaked cotton swab on each film, cellulose redisperses and resettles when dry. Solvent affects the films as they can break, buckle, and roughen; these effects can prevent the deposition of different layers during PSC fabrication, especially the first ones. The test was adapted from the ASTM D5402 to judge the quality of organic coatings. The film

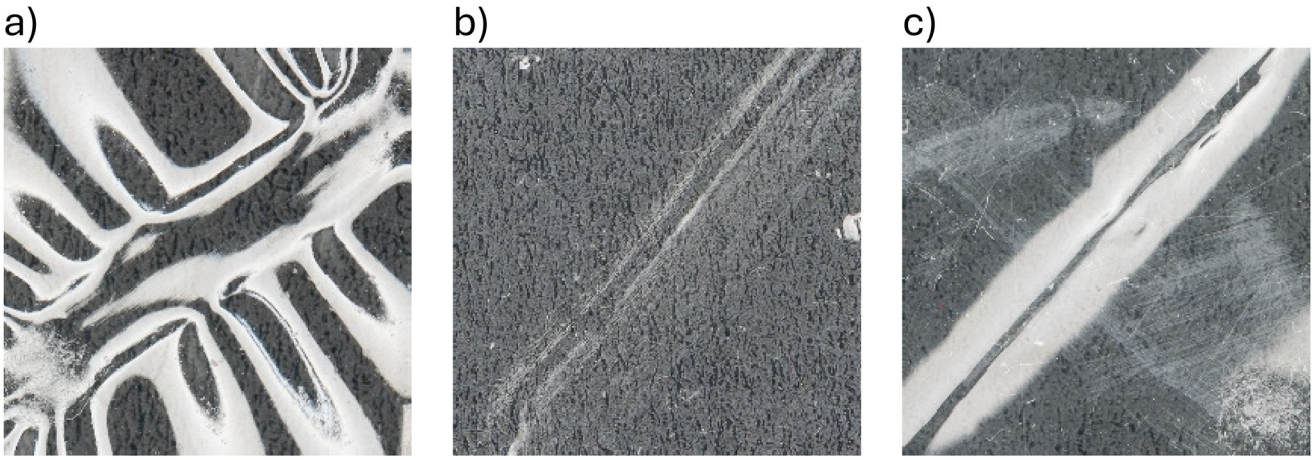

Fig. 4 Cellulose films affected by different solvents after being rubbed with a soaked cotton swab. The cellulose partially redissolved upon contact with the solvent, which affected the surface and structural integrity of the film. (a) Carboxymethylated cellulose rubbed with water, (b) cellulose acetate rubbed with dimethylformamide, and (c) ethyl cellulose rubbed with ethanol.

Table 3 Solvent resistance of different types of cellulose. An X indicates a noticeable change in film appearance caused by contact with a solvent

Solvent	Carboxymethylated cellulose (CMC)	Cellulose nanocrystals (CNC)	Cellulose acetate (CA)	Ethyl cellulose (EC)	Hydroxyethyl cellulose (HEC)	Cellophane
Water	✗	✗	✓	✓	✓	✓
Ethanol	✓	✓	✓	✗	✗	✓
Isopropanol	✓	✓	✓	✗	✗	✓
Acetone	✓	✓	✗	✗	✓	✓
Methanol	✓	✓	✓	✓	✗	✓
γ-Valerolactone (GVL)	✓	✓	✗	✓	✓	✓
Dimethyl sulfoxide (DMSO)	✓	✓	✗	✗	✓	✓
γ-Butyrolactone (GBL)	✓	✓	✗	✗	✓	✓
Dimethylformamide (DMF)	✓	✓	✗	✗	✓	✓
Chloroform	✓	✓	✓	✗	✓	✓
Chlorobenzene	✓	✓	✓	✗	✓	✓
1,2-Dichlorobenzene	✓	✓	✓	✗	✓	✓
Toluene	✓	✓	✓	✗	✓	✓
Diethyl ether	✓	✓	✓	✗	✓	✓
Acetonitrile	✓	✓	✓	✗	✓	✓

preparation description along with pictures for every entry, in line with Fig. 4, can be found in the SI, Table S1.

The first solar cell layers are prone to damaging the cellulose directly. Particular attention needs to be paid to the solvent compatibility of the first layers that could come in contact with cellulose. For example, the first layer may be too thin or too porous and thus allow solvents to reach the substrate and damage it. A type of cellulose that can withstand all the solvents used should ideally be chosen, or the cellulose should be crosslinked to increase its solvent resistance.

Crosslinking for improved solvent resistance. Crosslinking is the process of chemically or physically linking two or more different polymer chains to create an interconnected network. Physical crosslinking arises from electrostatic interactions between the polymer and the crosslinker, whereas chemical crosslinking involves the crosslinker reacting with the polymer chain to create a covalent bond. Films made through chemical crosslinking exhibit better tensile strength and formability and absorb less water than films made through physical crosslinking, but at the expense of lower elongation.[48]

In the case of cellulose, a molecule or a short polymer chain bonds two parallel cellulose chains and prevents them from redispersing or redissolving, thus granting cellulose films solvent resistance and/or modifying their properties. Crosslinking occurs along the active sites on the cellulose chains, which can be hydroxyl groups or other functional groups, and depending on their nature, a catalyst might be required. For instance, 1,2,3,4-butanetetracarboxylic acid (BTCA) has been used to crosslink cotton fibers and thereby obtain cotton fabrics with wrinkle and fire resistance. It can also be used to increase the water resistance of cellulose films (Fig. 5). Cellulose nanofiber (CNF) films crosslinked with BTCA remained stable in water even when submerged for 5 months. Sodium hypophosphite (SHP) is used as a catalyst for hydroxyl radical reactions in both cellulose and BTCA.[49]

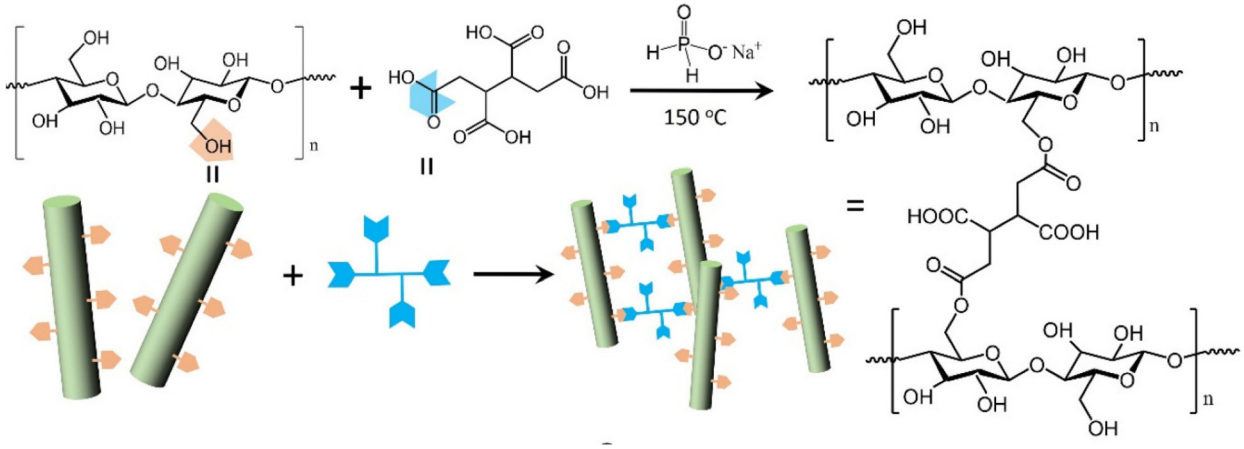

Fig. 5 Crosslinked cellulose with BTCA, adapted from ref. 49 with permission from Elsevier.[49] Copyright 2021.

A similar approach can be taken for hybrid films. For example, crosslinking CMC with cornstarch using epichlorohydrin (ECH) results in water-resistant films. ECH reacted and simultaneously bonded with CMC and starch active sites to form 3-propyleneglycol, which acts as a plasticizer that increases the resulting films' flexibility.[50] However, ECH is quite toxic, and a safer alternative is required. Citric acid is another small molecule that has been used to crosslink cellulose. Transparent films made of regenerated bacterial cellulose can be crosslinked with citric acid without a catalyzer, although this process is carried out in toxic *N*,*N*-dimethylacetamide.[51] This solvent can potentially be replaced by safer ionic liquids or deep eutectic solvents.[52]

Crosslinking can also be catalyzed using UV light. EC can be crosslinked with ethoxylated trimethylolpropane triacrylate through UV light to obtain films with increased solvent resistance and tensile strength. These films have been used as substrates in organic solar cells (OSCs) with almost 19% efficiency.[31]

Decreasing thermal expansion. Substrate expansion and contraction during thermal annealing occur due to a mismatch between the layers' coefficients of thermal expansion and can damage subsequently deposited layers.[53] Therefore, it is advisable to use substrates with very low CTEs or minimize the annealing temperatures and times. Synthetic polymer substrates have high CTEs[28,29] compared to flexible glass,[54] which is among their biggest flaws. The CTE of cellulose depends on the cellulose chain direction, giving different values depending on the geometric dimension that is measured.[27,53] The CTE decreases when the cellulose network is crosslinked, as this reduces thermal expansion.[55] Table 4 presents the CTE values for PSC substrate materials.

Although CTE is an important property that highlights the suitability of cellulose as a substrate material for optoelectronics, it is seldom reported in the literature and requires further research. It is unclear whether the cellulose moisture content has an effect on CTE and, if so, to what extent. Table 4 also includes the testing conditions used to obtain CTE values. There seems to be no apparent standard way to measure CTE between different materials. It would be useful to report the percentage of thermal expansion similar to how Nishino *et al.* do in their work.[26] This approach would be useful to determine if there is a difference in CTE due to water loss and plasticizer degradation.

Plasticizing for more flexibility. Depending on the cellulose type and film thickness, cellulose films can be quite brittle, which hinders their adoption. Although reducing their thickness can increase bendability and optical transmittance, it comes at the expense of an increased OTR and WVTR. Adding a plasticizer is a common approach for increasing the flexibility of bioplastics. Tensile strength, water vapor and oxygen permeability values (WVP and OP, respectively) can be found in Table 5.

Glycerol is a well-known plasticizer in the cellulose field due to its chemical similarity. It interacts with hydroxyl radicals and reduces hydrogen bonding between cellulose chains, which reduces the interactions between chains when the films are bent, thereby increasing their flexibility.[61] The higher the plasticizer concentration in a film, the more space it occupies between the polymer chains and the greater the flexibility.[62] Glycerol is compatible with many cellulose derivatives, such as CMC,[61] CA,[62] microcrystalline cellulose,[46,63] and CNC.[64] The effects of glycerol's interactions with hydroxyl groups vary depending on the cellulose radical groups and DS.

While glycerol is a good plasticizer, it is also known for increasing OTR and WVTR. Research showed that mixing glycerol with other polyols, such as maltitol and sorbitol, can greatly decrease CNC films' gas permeability (from 2601 to 97 g μm m^{-2} day^{-1} for water and from 134 to 20 cc μm m^{-2} day^{-1} for oxygen) while maintaining good flexibility.[65] Maltitol, in particular, was proved to increase CNC films' elongation at break to levels similar to PET and other plastics, and it has the added benefit of increasing optical transmittance while decreasing surface roughness.[66]

Additives to lower the OTR and WVTR. When used as PSC substrates, cellulose films should be able to withstand long-

Table 4 CTE for different substrate materials

Material	CTE [ppm K^{-1} or 10^{-6} °C^{-1}]	Testing conditions	Ref.
FG	0.31	Unspecified	54
Steel foil	16	Taken from the literature	56
Titanium foil	8.9	Taken from the literature	56
PET	15–117	A thermal expansion analyzer (TMA 402 F3, NETZSCH, Germany) was used to evaluate the CTE of the TSV sample at a heating rate of 10 °C min^{-1} in the range of 10–100 °C under nitrogen flow Commercial sample The CTEs of samples measuring 20 mm long and 20 mm wide were evaluated using a thermal expansion analyzer (NETZSCH DIL 402 C, Germany). The measurements were conducted three times from 25 °C to 100 °C by elevating the temperature at a rate of 10 °C min^{-1} under an inert gas atmosphere and taking the average value	28–30
PEN	13–20	Commercial sample	29 and 53
Polyimide (PI)	12–60	A thermal expansion analyzer (TMA 402 F3, NETZSCH, Germany) was used to evaluate the CTE of the TSV sample at a heating rate of 10 °C min^{-1} in the range of 10–100 °C under nitrogen flow Commercial sample	28, 29 and 53
Polycarbonate (PC)	60–122	Commercial sample The CTEs of samples measuring 20 mm long and 20 mm wide were evaluated using a thermal expansion analyzer (NETZSCH DIL 402 C, Germany). The measurements were conducted three times from 25 °C to 100 °C by elevating the temperature at a rate of 10 °C min^{-1} under an inert gas atmosphere and taking the average value	29 and 30
Cellulose microfiber composite	0.17	Measured with a TMA-SS120S (Seiko Instruments). Heating rate of 10 °C min^{-1}. The specimen with an original length of 15 mm was subjected to a uniaxial stress of 0.12 MPa	26
Microcrystalline cellulose crosslinked with epichlorohydrin	6.9	Measured with a thermomechanical analyzer (TMA-SS6100, Seiko Instruments)	55
Self-organized CNC (self-organized/shear-organized)	~25/9–158	Digital image correlation (DIC) methodology used. Images were captured at 25, 40, 60, 80, and 100 °C. A 10 min stabilization time was allowed at each temperature before capturing images	27
CNC	2.7	Atmospheric condition of nitrogen and heating rate of 5 °C min^{-1}, calculated over the specified regions from 50 to 150 °C and each 5 °C range	57
CNC/CNF	11.86–17.65	The temperature used in CTE tests was increased from 20 to 120 °C at a rate of 3 °C min^{-1}	58
CNF	8.5	Measured using a thermomechanical analyzer (TMA/SS6100, SII nanotechnology Inc.). Specimens were 25 mm long and 3 mm wide with a 20 mm span. The measurements were carried out three times with a heating rate of 5 °C min^{-1} under a nitrogen atmosphere in tensile mode under a load of 3 g. The CTE values were determined as the mean values at 20–150 °C in the second run	59
CMC	38	Measured using a TMA Q400	60
CA	55.3	Commercial sample	53
Cellophane (flow direction/transverse direction)	18.2/33.6	Commercial sample	53

term exposure to external environmental conditions to maintain a good PCE as well as prolong the lifetime of the device. It is well known that most cellulose films are susceptible to air and moisture damage. Therefore, the air and humidity barrier properties of cellulose films must be considered and carefully tested using standard protocols. The OTRs and WVTRs of microcrystalline cellulose (MCC) film and different commercial materials of similar thickness were compared in a recent study.[68] The ASTM F3136-15 standard testing method was used to measure the oxygen uptake of samples as a function of time at 25 °C, 50% RH and thereby calculate OTR. The OTR of an MCC film with 20% naringin content (named CN-20) was 55 mL m^{-2} day^{-1} and significantly lower than the 310 mL m^{-2} day^{-1} OTR of pure MCC film. Guzman-Puyol *et al.* suggested that the antioxidant properties of naringin molecules limited the permeability of oxygen through the MCC film. The OTR of CN-20 was comparable to PET and polylactic acid (PLA) films of similar thickness.[68] WVTR determination was subsequently conducted in accordance with the ASTM E96 protocol. Each film was mounted on top of a permeation cell in a 0% RH desiccator, and water was passed through it. The WVTR of the CN-20 film was approximately 3000 g m^{-2} day^{-1}, closest to that of polystyrene (PS) films. Some commercial substitutes, such as PET, LDPE, and nylon 6 possess even lower WVTR values. Nonetheless, these results support the application of modified cellulose-based films with promising oxygen and water barrier properties.

Different cellulose types have been combined to study the resulting synergistic effects on their barrier and mechanical properties. Fernández-Santos *et al.* tested CNC films with varying proportions of CNF and CMC.[69] At 90% RH, CNC films with more than 40% CMC showed increased resistance to

Table 5 Plasticized cellulose films with improved mechanical and gas barrier properties

Material	Plasticizer	Tensile strength (MPa)		WVP (g μm (m^2day)$^{-1}$) (23 °C, 50% RH)		Oxygen permeability (OP) cm^3 μm m^{-2} day^{-1} (23 °C, 50% RH)		Ref.
		Without plasticizer	With plasticizer	Without plasticizer	With plasticizer	Without plasticizer	With plasticizer	
CNC	Glycerol	62.3	32.9	2601	2669	134	494	65
CNC	Sorbitol	62.3	39.2	2601	399	134	153	65
CNC	Maltitol	62.3	47.5	2601	97	134	29	65
CNC	Maltitol	64.2 ± 10.9	32.4 ± 2.3	6.06×10^{-11} g Pa^{-1} s^{-1} m^{-1}	3.67×10^{-12} (g Pa^{-1} s^{-1} m^{-1})	21.68 cm^3 μm m^{-2} day^{-1} atm^{-1}	4.75 cm^3 μm m^{-2} day^{-1} atm^{-1}	66
CA	Glycerol and triethyl citrate	34	8	1.0×10^{-4} g Pa^{-1} s^{-1} m^{-1}	7.0×10^{-5} g Pa^{-1} s^{-1} m^{-1}	—	—	67
Regenerated cellulose crosslinked with Ca^{2+}	Glycerol	4.5 ± 4	0.8 ± 4	$1.48 \pm 3 \times 10^{-8}$ g Pa^{-1} s^{-1} m^{-1}	$10.12 \pm 9.65 \times 10^{-8}$ g Pa^{-1} s^{-1} m^{-1}	—	—	63
Regenerated cellulose crosslinked with Ca^{2+}	Sorbitol	4.5 ± 4	0.3 ± 1	1.48×10^{-8} g Pa^{-1} s^{-1} m^{-1}	$1.08 \pm 10 \times 10^{-10}$ g Pa^{-1} s^{-1} m^{-1}	—	—	63

water vapor, hence lower WVTR values which rapidly reached those of pure CMC of 3.38 g m^{-2} day^{-1}. CMC contributed to better water resistance by forming dense, compact networks, whereas the free –OH groups and crystals of CNF led to higher water vapor permeation and reduced barrier water properties. Similar findings on the effects of CMC and CNF were also obtained by another research group.[70] Pure cellulose films could be fine-tuned to obtain oxygen and water barrier properties that exponentially increase PCE and device stability. These properties are especially desirable for PSC application in humid conditions.

CMC films combined with sodium montmorillonite (Na-MMT) nanoclay exhibited a 39% reduction in water vapor permeability compared to pristine CMC films.[71] This enhanced water barrier property could be attributed to the formation of strong hydrogen bonds between the –OH groups of CMC and Na-MMT, which hinder the availability of –OH groups for moisture absorption. The incorporation of TiO_2, which has inherent UV-shielding properties, led to a further decrease in water vapor permeability by 50%. CMC films comprising 5 wt% Na-MMT and 1 wt% TiO_2 had good tensile strength (6.18 ± 2.01 MPa) and Young's modulus (28.93 ± 5.74 MPa) but became non-transparent. Thus, nanocomposite CMC films would require further optimization to be employed as substrates in PSCs. In our previous work, we explored the use of montmorillonite clay (MMT) to produce transparent films (60–80% at 550 nm) with improved gas barrier properties. We found that MMT induces some improvements in the barrier properties,[72] but they are far from what is needed for stable PSCs; the required levels for PSCs range from 10^{-3} to 10^{-6} g m^{-2} day^{-1} for WVTR, and from 10^{-2} to 10^{-5} cm^3 m^{-2} day^{-1} for OTR.[73] Thus, a separate protective coating is needed to achieve acceptable gas barrier levels (see Coatings to increase barrier properties section). WVTR and OTR values for some PSC substrate materials are given in Table 6.

Step 2: casting cellulose films

Simple casting is the most common approach for cellulose film production. This involves dissolving cellulose in a suitable solvent at specific concentrations, followed by intensive stirring until a homogeneous solution is obtained, which is then cast on a container and left to dry. Many variables can affect the resulting film's characteristics, such as the cellulose concentration in solution, solvent type, shape and surface of the container, and drying temperature and environment.

In our previous work on CNF films, we demonstrated that films made with CNF suspensions with lower concentration led to higher transparency levels and lower surface roughness.[78] This was attributed to the increase in cellulose agglomerates in high cellulose concentrations. Similarly, the solvent choice can also impact film formation. Changing the solvent from acetone to *N*-methyl-2-pyrrolidone (NMP) was shown to have an overall positive impact on composite CA and CNF film formation, specifically by increasing the films' transparency and mechanical strength and lowering their surface roughness

Table 6 WVTR and OTR levels for different flexible substrate materials

Material	Thickness [μm]	WVTR [g (m^2 day)$^{-1}$]		OTR [cm^3 (m^2 day)÷]	Ref.
		Without modification	With modification		
FG (NEP G-Leaf™)	30–700	—	Below 1 × 10^{-5} detection limit	Below 1 × 10^{-2} detection limit	74
PET	100	—	3.9–17	1.8–7.7	75
PEN	100	—	7.3	3	75
PI	100	—	0.4–21	0.04–17	75
CMC crosslinked with CA	50–100	33.8	Less than 0.02 g mm m^2 day^{-1}	—	76
CNF with montmorillonites (MMT) clay and polyethylenimine (PEI)	35 ± 3	30 wt% ML-MMTs: 41.5 O-MMTs-CNFs: 78.7	20.9 g mm m^2 day^{-1}	—	77

and water absorption.[79] These improvements can be explained by CNF's increased dispersion in NMP compared to acetone.

The container used for casting has a big influence on film transparency. Cellulose films cast on hydrophobic surfaces are denser, more transparent, and have lower WVTR and higher tensile strengths than films cast on hydrophilic substrates.[80] As the suspension on hydrophilic surfaces dries, the cellulose fibers sediment and form random fiber networks. On hydrophobic surfaces, the solvent experiences tension due to its interaction with the container, and capillary forces drive the fibers to align, ultimately resulting in high transparency.

The drying conditions have a notable impact on film formation too. In the case of CNF films, hot press drying has been found to increase mechanical strength, lower oxygen and water vapor transmission rates, and lower surface roughness, primarily due to the improved consolidation of the CNF layers.[81] In the case of EC, drying at 6 °C produces better films than drying at room temperature, even with added plasticizers.[82] In the case of CA, humidity greatly affects film transparency and uniformity.[83] The slow and gradual evaporation of the solvent is believed to be one of the main parameters contributing to high-quality films with both EC and CA.

Surface roughness. In optoelectronics, surface roughness is an essential parameter for evaluating substrates and deposited layers. Since some layers can be very thin (around 10 nm), high surface roughness can lead to poor surface coverage and even cause short circuits if conductive materials protrude into other layers; as such, the aim is always to try and minimize surface roughness. The roughness values of different electrode materials are listed in Table 7.

The surface roughness of cellulose films greatly depends on the casting surface.[84] Cellulose chains assemble while the film dries and thus roughly adopt the container's surface roughness, so it is prudent to use the smoothest container possible. Some types of cellulose, such as CMC, EC, and CA, peel off easily from glass containers, whereas CNC and CNF films remain firmly attached to hydrophilic surfaces. For the latter, it is ideal to use plastic containers or to treat hydrophilic surfaces (like glass) with a hydrophobic coating. Many of these coatings are highly toxic siliconizing agents, so caution is advised.

A film's roughness may be very high even after using a smooth substrate. In such cases, films can either be coated with a planarization layer or hot pressed. Depositing SiN_x on CNF films has been shown to reduce the surface roughness to 1 nm and provide the added benefit of greatly reducing the WVTR to less than 0.02 g m^{-2} day^{-1}.[85] Alternatively, CNF films can be hot pressed at 120 °C for 10 min at 1.1 MPa.[81] Hot pressing is mainly useful for films with very high roughness, as it helps to reduce roughness on a macro level.

Table 7 Surface roughness for different electrodes on different substrate materials

Material	Surface roughness (R_q) [nm]	Ref.
Glass/ITO	2.15	86
Glass/FTO	45.43	86
Glass/polished FTO	14.96	86
FG/ITO	4.3–30.3	87
Titanium foil	25.34	88
Stainless steel foil (untreated and polished)	57.4, 25.2	89
PET/ITO	1.8–4.4	90
PEN/ITO	4.66	91
Hydroxypropyl methyl cellulose/AgNWs	7.07	92
Nanocellulose paper/PEDOT:PSS	6.54	14

Coatings to improve barrier properties. As mentioned earlier, the additives in pure cellulose films fail to provide sufficient protection against oxygen and water (see section Additives to lower the OTR and WVTR) and need to be supplemented with barrier coatings. Modified CA films with excellent oxygen and moisture barrier properties (77.0–26.3 g m^{-2} day^{-1}) and good transparency were recently reported to be promising substitutes for PET films.[93] When cross-linked with pyromellitic dianhydride (PMDA) and hydrophobized using tetraethyl orthosilicate (TEOS) and octyltrichlorosilane (OCTS), these CA films exhibited improved solvent resistance (acetone and DMSO) and mechanical properties. Other ceramic coatings have also shown different degrees of success, as given in Table 8.

Castro-Hermosa *et al.* have reported that low gas barrier levels are expected for PSCs,[73] outside the current range for modified cellulose films, but their discussion about gas barrier properties is focused on encapsulated devices and not solely on the substrate. For instance, thermoplastic starch

Table 8 Coatings that reduce gas penetration in cellulose films

Material	Thickness [μm]	WVTR [g (m^2 day)$^{-1}$] (23 °C and 50% RH)		OTR [cm^3 (m^2 day)$^{-1}$]		Ref.
		Without coating	With coating	Without coating	With coating	
CA crosslinked with PMDA and coated with OCTS	153–215	77.0 ± 2.5	29.5 ± 1.7	280 (23 °C and 80% RH)	24.6 ± 0.8	93
CNF coated with SiN_x	41.4	13.60 ± 0.42 (38 °C and 50% RH)	Below 0.02 detection limit	10.83 ± 0.99 cm^3 m^{-2} day^{-1} bar^{-1} (70% RH)	—	85
Paper coated with Al_2O_3 through atomic layer deposition	60	589.9 ± 15.1	2.2 ± 0.5	—	—	94
Cellophane coated with SiOx	35	65.85 (23 °C and 85% RH)	1.28	10.44 (23 °C and 0% RH)	0.82	95

(TPS) films reinforced with CNF have OTR levels below 2 × 10^{-4} cm^3 m^{-2} day^{-1} and WVTR levels below 2.24 × 10^{-2} g (m^2 day)$^{-1}$ and still maintain an optical transmittance of over 80% at 550 nm.[96] Films like these have relatively high surface roughness levels, and their resistance to the solvents used in PSCs is yet unclear. It could be possible to combine PSCs made on cellulose films with a TPS/CNF encapsulant, using transparent biobased materials for both the substrate and the encapsulant.

Step 3: depositing the bottom electrode

FTO and ITO, the most typical electrode materials for PSCs, face issues when combined with cellulose. The use of FTO is limited to glass substrates due to its high-temperature processing requirements, and while ITO can be sputtered at low temperatures, indium is a scarce element. More sustainable electrodes are being investigated. Among them, conductive polymers and metallic nanowires have been shown to be compatible with cellulose. A comparison of various electrode materials and substrates is presented in Table 9.

Poly(3,4-ethylenedioxythiophene) (PEDOT) is a well-investigated conductive polymer whose sheet resistance can reach around 20 Ω sq.$^{-1}$,[97] close to the usual values of TCO. However, a notable drawback is that thick layers of PEDOT are required to achieve low resistivity, which significantly reduces its transparency. PEDOT's conductivity can be greatly increased by doping and crosslinking the polymer. Polystyrene sulfonate (PSS) is a common dopant used to increase the conductivity of PEDOT and simultaneously decrease electrode thickness and increase transparency. With the addition of a conductivity and flexibility enhancer (CFE), PEDOT:PSS:CFE can reach conductivities of over 4100 S cm^{-1} and a transmittance of 85%, comparable to commercial ITO on PET. Perovskite solar modules consisting of this electrode were shown to reach 10.9% PCE on a 25 cm^2 active area.[98] PEDOT and PEDOT:PSS are compatible with cellulose, as PEDOT evaporates at low temperatures, and PEDOT:PSS can be spin coated or printed. Their inks are usually water-based, which means that water-resistant cellulose is required (see Table 3).

N-doped poly(benzodifurandione) (*n*-PBDF) is a novel polymer electrode made as a TCO alternative. Similar to PEDOT:PSS, it is solution-based and can be deposited at low temperatures *via* spin coating, inkjet printing, blade coating, and spraying. Sheet resistances 90.9 and 78.8 Ω sq.$^{-1}$ can be obtained by spraying layers of 65–75 nm thickness. $FAPbI_3$ PSCs were built on PET/*n*-PBDF substrates with 11.24% PCE.[99]

Metallic nanowires have gained interest as promising ITO substitutes due to their excellent features, which include low sheet resistance, high transparency, and easy deposition *via* spraying or spin coating. Their high transparency stems from the random deposition of nanowires and the resulting mesh-like structures, leaving holes through which light can travel. Silver nanowires (AgNWs) are the most commonly used nanowires thanks to their high conductivity of around 12 Ω sq.$^{-1}$ and 94.4% transmittance,[100] although more sustainable options such as copper[101,102] and nickel[103] are also being investigated. To attain high conductivities, electrical losses need to be reduced by welding nanowire junctions *via* thermal annealing,[104] laser sintering,[105] or chemical processes.[106,107]

Poor substrate bonding strength and high surface roughness are the major disadvantages of metallic nanowires. Addressing these typically requires nanowires to be embedded in a different material, either by pressing the material into the substrate[107] or by mixing the two in a conductive material matrix to improve conductivity.[108] One way to solve both of the aforementioned issues when working with cellulose is to spray the nanowires on a rigid surface and then cast the cellulose. This greatly reduces the surface roughness and keeps the nanowires from moving inside the cellulose film (Fig. 6).[109]

Table 9 Different electrode materials for solar cells

Conductive substrate	Thickness [μm]	Transmittance [%]	Sheet resistance [Ω sq.$^{-1}$]	Ref.
FG (Corning Willow Glass)/ITO	100	~80 (at 550 nm)	12.6 ± 0.1	111
Titanium foil	—	0	~3.6	112
Stainless steel foil	—	0	<0.5	113
PET/ITO	188	80–90 (at 550 nm)	14.5–17.3	90
PEN/ITO	125	~82 (at 550 nm)	15	
EC/AgNWs	8	88 (400–1000 nm)	21.04	31
Cellophane/TiO_2/Ag/TiO_2	—	82.1 (400–800 nm)	9.5	114

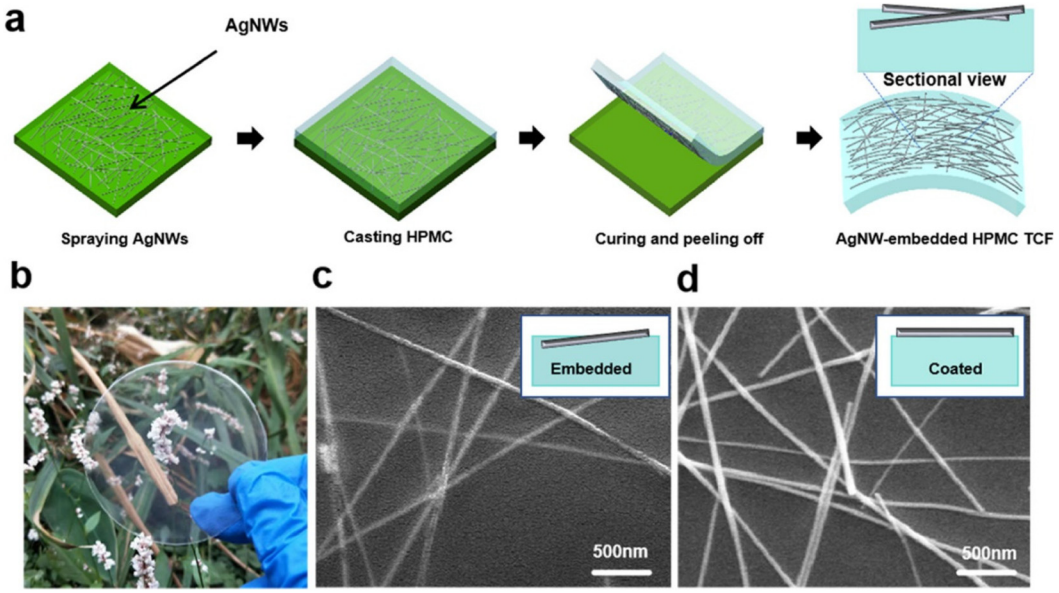

Fig. 6 Pre-patterned AgNWs embedded in a hydroxypropyl methyl cellulose film. (a) Fabrication procedure, (b) photograph of the cellulose film embedded with nanowires, (c) SEM micrograph of film with embedded nanowires, (d) SEM micrograph of film with coated nanowires, reproduced from ref. 109 with permission from the American Chemical Society.[109] Copyright 2020.

AgNWs were used as electrodes on cellulose to make OSCs, with an impressive 18.71% efficiency level,[31] proving that cellulose is suitable for the development of high-efficiency devices.

The highest-performing PSC made on cellulose was made using an oxide/metal/oxide electrode (OMO), specifically TiO_2/Ag/TiO_2, and reached 13.19% PCE.[36] Devices made with OMO electrodes were made using $MAPbI_3$, which partly explains their low performance compared to lower bandgap perovskites. The OMO electrode was sequentially sputtered and reached a sheet resistance of 3.6 Ω sq.$^{-1}$, well below the 30 Ω sq.$^{-1}$ of commercial PET/ITO but with similar optical transmittance.[110] OMO electrodes have the advantage of being easy to deposit, but due to the need for vacuum deposition, their scalability would depend on a high initial investment compared to wet methods.

Using a carrier substrate. The most common fabrication methods used in laboratories, such as spin coating, are designed for rigid substrates. While there are attachments available for the use of flexible substrates in spin coaters, synthetic polymers and cellulose tend to bend, buckle, expand, and contract because of tension on the films, moisture, or during thermal annealing. Therefore, it is advisable to attach cellulose films to a carrier substrate such as glass during processing. Double-sided tape, glue, and adhesive gels are the most common adhesives for this application. In R2R processes, cellulose films can be attached to flexible carrier substrates, such as PET or some other polymer film.

When attaching a film to a carrier, there are many things to consider. First, the carrier and the adhesive surface should be as smooth as possible to prevent protrusions that could compromise the cellulose surface, which would, in turn, affect the deposition quality of the subsequent layers. Second, an adhesive with an adequate thermal resistance must be chosen based on the highest temperature expected during PSC processing. Third, if the device is to be characterized while it is on the carrier, the optics of the adhesive have to be considered, as these will impact how much light reaches the active area. Fourth, if bending tests are to be done, the device needs to be peeled off the carrier without being damaged.

Step 4: solvent washing

Conventional glass and plastic substrates are normally washed with ultrasonication baths in different solvents.[45] In laboratory settings, the quality of the deposited layers is ensured by washing the substrate to eliminate all the loose particles on its surface and leftovers from the etching process, such as zinc remnants and the Kapton tape adhesive. Substrates are washed in a soap water bath, followed by an acetone bath and an isopropanol bath, and then dried with nitrogen gas. For applications that require high hydrophilicity and no traces of organic components, the substrates are subjected to a chemical bath in a piranha solution. This mixture of sulfuric acid and hydrogen peroxide decomposes most organic matter and is, therefore, unsuitable for synthetic polymers and cellulose films.

For small-scale spin-coating processes, a compatible solvent is dynamically spin coated at high speed over a cellulose film to clean the surface. In large-scale R2R fabrication processes, the substrates are washed with an organic solvent, such as isopropanol or ethanol, followed by an air plasma corona treatment. Web cleaning may also be performed, which involves using rolls made of a sticky elastomer to remove dust particles from the substrate surface.[115,116] Substrates can also undergo

UV-O_3 or plasma treatments, as discussed below (see section Step 5: wettability).

Cellulose is compatible only with some of these cleaning methods; ultrasonication in a solvent bath risks cellulose redispersal in the solvent. The recommended approach is to dynamically spin coat a compatible solvent (*i.e.*, something that would not redissolve the film) quickly, spray the substrate surface with N_2, and treat the film inside a plasma cleaner. Web cleaning and corona treatments are suitable methods for removing dust and cleaning the cellulose surface in large-scale processes.

Step 5: wettability

In many cases, the surface that needs to be coated has poor wettability, which prevents the ink from completely covering it. To address this issue, surfaces are typically subjected to UV-O_3 or plasma treatment. These treatments have a dual purpose: to remove organic matter left on the surface after cleaning and to increase the surface wettability. Surfactants can also be used instead of surface treatments to increase the ink's spreadability over the substrate.

UV-O_3 and plasma treatments. UV-O_3 cleaners consist of mercury lamps that produce UV light in the 254, 302, and 365 nm wavelengths, which correspond to UV-C, UV-B and UV-A, respectively. These wavelengths allow for sanitizing surfaces and liquids, killing bacteria. Ozone-producing lamps work by producing 185 nm light, which splits molecular oxygen (O_2). These oxygen atoms react with more O_2 to form an ozone molecule (O_3). Next, the 254 nm light splits the O_3, and the resulting ions react with the substrate surface to break down the organic residues on the surface into volatile components and ionize the substrate surface, thus increasing its wettability.[117] UV-O_3 is a common surface treatment used in solar cell fabrication processes to clean and increase the wettability of ITO, FTO, and ceramic layers such as TiO_2, SnO_2, ZnO, and NiO_x.

UV exposure has been shown to increase cellulose swelling and reduce the material's mechanical properties.[118] These effects occur because bond scissions between glucose units in the cellulose chains create more sites to form hydrogen bonds with water, as evidenced by the reduced cellulose chain length.[119] UV light can penetrate the cellulose bulk and greatly increase the material's hydrophilicity, in addition to affecting the surface. This could prove disadvantageous when using cellulose substrates, as inks would get absorbed into the substrate and prevent layers from forming on top.

Another common technique for surface cleaning involves the use of plasma. An electric current is passed through a gas to ionize it, and these ions bombard the substrate surface, resulting in etching or an increase in bonding attributes. When the plasma exposure energy is low, this effect is confined to the substrate surface and affects only the top molecular layers, not the bulk, reaching a depth of around 4–6 Å.[120] Gas ionization is controlled by applying an energy field at radio frequencies around 13.56 MHz, as these have been found to produce homogeneous results.

Since cellulose is often a porous material, an increase in its hydrophilicity can render cellulose films absorbent. This is undesirable, as the material would then absorb the solutions used to make layers on top of it. Similar to UV-O_3 treatment, plasma can break the molecular oxygen bonds to form free oxygen radicals. However, plasma only affects the substrate surface and is thus more suitable than UV-O_3.

A useful alternative to surface treatments is to include a surfactant to reduce surface tension and facilitate the deposition of inks in a controlled manner. When PEDOT:PSS is used as an electrode, Tween-80 can be used to improve its spread over glass, without any surface treatment. This approach has the benefit of decreasing PEDOT:PSS sheet resistance to 202 Ω sq.$^{-1}$ (ref. 121). When used as an HTL, PEDOT:PSS has a tendency to corrode the perovskite layer, which greatly decreases the perovskite stability. Triton-X 100 (TX) can be used to increase the spreadability of PEDOT:PSS and insulate the perovskite, which would, in turn, lead to reduced charge interface recombination. This method has been shown to increase PCE from 11.12% to 16.23%.[122]

TX can also be used to greatly reduce the surface tension of SnO_2 nanoparticle (NP) inks intended for R2R processes. Excessive TX acts as an impurity and decreases device performance, so isopropanol (IPA) is mixed with water to further decrease the surface tension.[123] Alternatively, SnO_2 can be mixed with polyethylene oxide–polypropylene oxide–polyethylene oxide (P123) to increase the ETL spread, compactness, and uniformness. This dopant also increases device stability, thanks to the increased binding interaction between SnO_2 and the perovskite layer, and 85% of the initial performance is retained after 1000 h of storage in air.[124]

Step 6: depositing the first CTL

Depending on the chosen device architecture, namely NIP or PIN, an n-type or a p-type semiconductor material is deposited on top of the bottom electrode. TiO_2 is the most commonly used ETL—a legacy from dye-sensitized solar cells when perovskite was discovered as a photoactive material.[125] Mesoporous titania (m-TiO_2) acts as a scaffold for the perovskite; both materials remain in close contact, enabling charge separation and electron transport to the bottom electrode. A thin layer of compact titania (c-TiO_2) is deposited before m-TiO_2 to better match the band levels between the perovskite, the ETL, and the bottom electrode. Both layers of TiO_2 need to be sintered at temperatures over 400 °C, outside the temperature range of synthetic polymers and cellulose.[45] Tin oxide (SnO_2) is an alternative to TiO_2 that can be annealed at very low temperatures; it is commonly sold as nanoparticles suspended in water[126] or can be made from tin chloride in ethanol.[127,128] ZnO may also be used as an ETL in PSCs, but it has been shown to degrade the perovskite quickly. Therefore, SnO_2 is the only viable low-temperature ceramic ETL so far. SnO_2 is typically annealed at temperatures between 150 °C and 180 °C,[129] although there are methods to anneal it at room temperature.[128,130] This is the highest temperature used for an annealing process during PSC fabrication, as the perovskite

layer is normally annealed at 100 °C.[45] It is also possible to top c-TiO_2 with SnO_2 for better band alignment and greater efficiency.[131]

Inverted structure devices have a wide range of options for their first CTL. Nickel oxide (NiO_x) is the most popular p-type HTL that is deposited on top of the bottom electrode. It can be deposited using various techniques, including spraying and sputtering, atomic layer deposition, and chemical baths. NiO_x has different stoichiometries depending on the deposition method, which affects its electrical properties and band alignment with the perovskite. Spin-coated NiO_x nanoparticles without annealing were used to make PSCs with 21.6% efficiency.[132]

Other than metal oxides, polymers have successfully been integrated into PSCs. PEDOT:PSS was the first polymer to be used as an HTL in inverted structure PSCs, and it can reach efficiencies of 19.19%.[133] Nonetheless, PEDOT:PSS significantly affects perovskite performance and stability due to its high hygroscopicity and acidity.[132] PSS corrodes the perovskite and provokes ion migrations to the ITO electrode. Substituting this dopant with hydrophobic poly(ethylene-*co*-vinyl acetate) (EVA) improves perovskite adhesion to the electrode and prevents ion migration, resulting in devices with efficiencies close to 20%.

Poly[bis(4-phenyl)(2,4,6-trimethylphenyl)amine] (PTAA) is another polymer used to make HTLs in inverted structure PSCs. It has the advantage of forming very smooth hydrophobic layers after annealing and is more stable than PEDOT:PSS.[132] However, these properties also lead to the perovskite solution dewetting too rapidly, resulting in nonuniform layers. This problem can be solved by using UV-O_3 or plasma treatment, but as discussed earlier, these treatments can damage organic layers. Researchers have opted to add surfactants to perovskite solutions to increase their spreadability. Dodecylammonium bromide (DDABr) proved to be a useful additive, resulting in PSCs with an impressive 24.3% efficiency, and up to 19.8% efficiency in 13.18 cm^2 aperture area devices.[134] PEDOT and PTAA can be deposited in a variety of ways; it is most apt to introduce these polymers in inks meant for printing or spraying.

The use of self-assembled monolayers (SAMs) has surged recently and has led to a variety of record-breaking PSCs, reaching efficiencies over 26% when combined with NiO_x.[135] Unlike PEDOT and PTAA, SAMs are small-sized molecules and are usually spin coated or sprayed onto the electrode or other CTLs. These molecules consist of three parts: an anchoring group that bonds the SAM to the substrate surface, a spacer group that determines the SAM tilt angle and connects the other two groups, and a terminal group that modifies the perovskite work function and inhibits interfacial charge recombination.[136] Each group can be adjusted based on the substrate surface and the influence on perovskite crystal growth, making them highly versatile. Their anchoring is driven by heat and is thus greatly affected by the substrate morphology; thus, the deposition technique needs to be optimized for different surfaces.[136]

Special care is required during this stage, as the charge transport material solvent can have a significant impact on the substrate. Thermal evaporation and sputtering have little effect on the substrate, but these processes are more expensive to implement in R2R processes. Printing, spraying, and slot-die coating all involve the use of solutions and inks, making the choice of material and solvent a critical issue at this stage (see Table 3).

Changing the solvents

Substituting water with ethanol. Commercial colloidal SnO_2, the most common ETL requiring low-temperature processing, is usually sold in water suspensions. This has a negative impact on water-soluble cellulose films (namely CMC and CNC; Table 3). One way to avoid water on this layer is to use SnO_2 on ethanol instead. SnO_2 can be synthesized from $SnCl_2{\cdot}2H_2O$ in ethanol. Specifically, $SnCl_2{\cdot}2H_2O$ reacts with ethanol to form $Sn(OH)_2$, which then decays into SnO and finally oxidizes to SnO_2.[128]

PEDOT:PSS is another popular PSC material that is sold in water. Water can be removed from the solution and replaced with ethanol through ultrafiltration and dialysis.[137] This approach has been used to make top electrodes for OSCs, reaching 14% efficiency.[138]

Step 7: first CTL thermal annealing

Many layers require thermal annealing in order to grow crystalline structures. TiO_2 is a very common ETL material, but its use is restricted to glass substrates because it requires annealing at 500 °C. New TiO_2 processing techniques have been developed to overcome this obstacle. Sputtering is one deposition technique that can be used at room temperatures and is scalable to high-volume fabrication. However, sputtered films normally require a thermal annealing process afterwards. To improve crystallinity and avoid high-temperature defects, sputtered TiO_2 films can be annealed using UV light. This method has produced PSCs with a remarkable PCE of 24.75% as well as perovskite modules on glass/FTO and PEN/ITO with PCEs of 18.82% and 14.61%, respectively.[139] It is also possible to deposit TiO_2 layers at room temperature using wet chemistry methods. For instance, a sol–gel titanium diisopropoxide bis (acetylacetonate) solution can be annealed with a laser at room temperature; this method has resulted in devices with 17.1% PCE on PEN/ITO substrates.[140]

SnO_2 is used instead of TiO_2 for the low-temperature processing of PSCs, yet it still requires temperatures over 150 °C to be annealed. Multiple approaches have been developed to overcome this. SnO_2 layers can be made using intense pulse light,[141] ultrasonic vibrations,[130] negative pressure,[142] UV light,[143] or amine fumes (Fig. 7),[128] and none of these methods require thermal annealing.

Nickel oxide is the most-used metal oxide HTL in PIN-structure PSCs. To overcome the need for high-temperature annealing, NiO_x NPs made with a tetramethylammonium hydroxide surfactant can be used. These require annealing at 150 °C, which is a more tolerable temperature than the normal annealing temperature of 400 °C. This fabrication method has resulted in PSCs with 18.85% PCE on glass/FTO.[144] Recently, a new HTL material known as DFBT-PMTP has been synthesized as an annealing-free and additive-free option for inverted

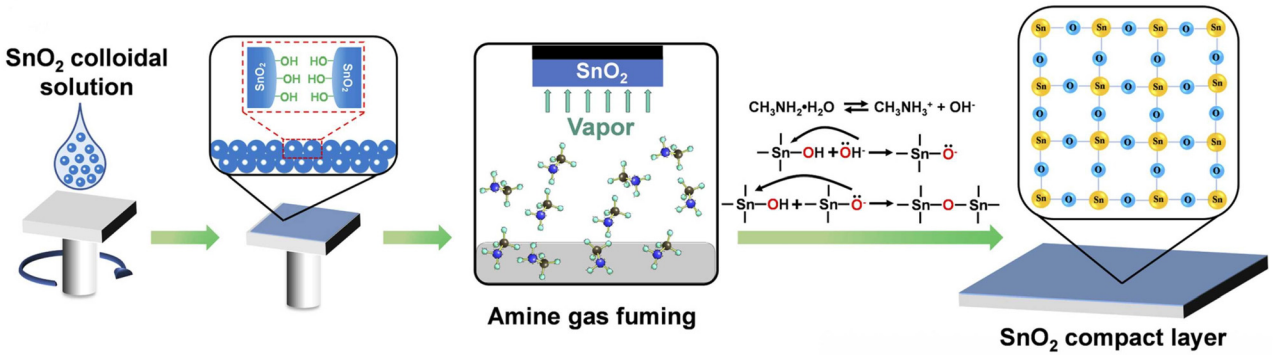

Fig. 7 Room temperature annealing of SnO_2 with amine fumes, adapted from ref. 128 with permission from Elsevier.[128] Copyright 2022.

PSCs; it has been shown to achieve 21.23% PCE.[145] SAMs such as MeO-2PACz can also be deposited as HTLs and annealed at temperatures below 100 °C to obtain high efficiencies without any thermal treatment.[146]

Step 8: perovskite deposition

Perovskite crystal formation is susceptible to temperature and solvent vapor changes in the environment. While there are ways to deposit the perovskite layer by evaporation, it is typically deposited with solution-based methods, as these are cheaper and easier to implement.[147,148] Perovskites have an ABX_3 structure, and different A cations and X anions are mixed to shift the perovskite band level and adjust the perovskite Goldschmidt tolerance factor. The A cations are usually small molecules such as methylammonium (MA) or formamidinium (FA) or big atoms such as cesium or rubidium. Iodine is the most common anion, followed by bromine and chloride.[149] The wet-method processing route consists of two different approaches for fabricating the perovskite layer—the one-step solution process (OSSP) and the two-step solution process (TSSP); both are illustrated in Fig. 8.

The OSSP involves mixing the perovskite precursors together in a single solution. When the precursors are deposited, the solvent needs to be removed to start the nucleation and crystallization of the perovskite layer. In spin coating, this is normally done by using an antisolvent, which removes the solvent from the substrate without redissolving the perovskite layer. In large-scale methods, the perovskite solvent choice is very important, as the solvent is removed using an N_2 air knife *via* the gas quenching method, and this is affected by

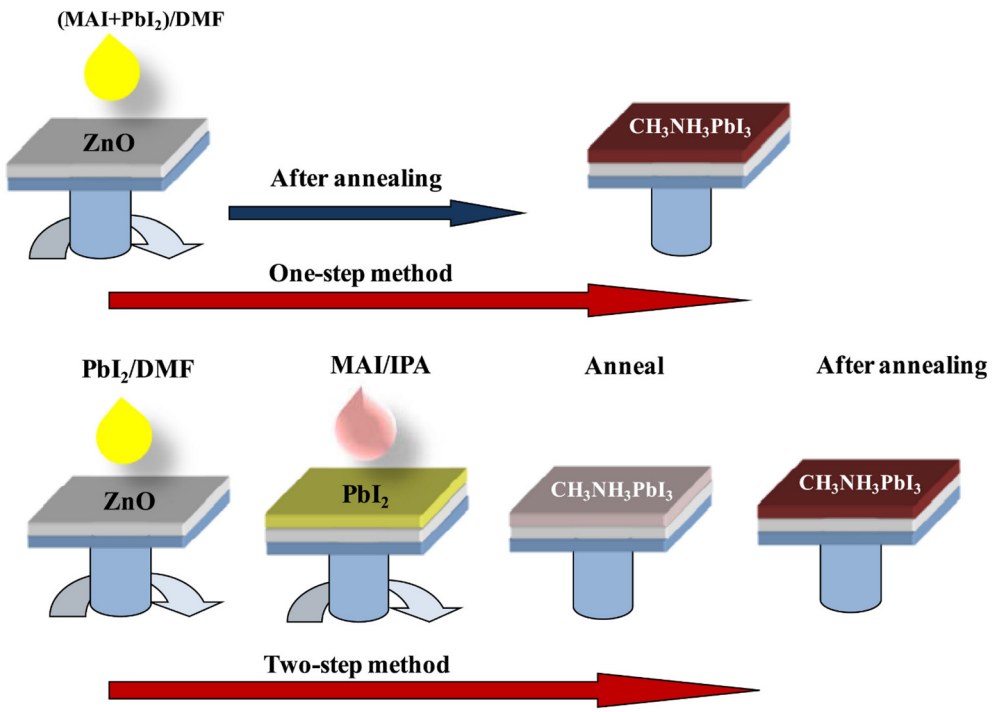

Fig. 8 Comparison of OSSP and TSSP, reproduced from ref. 150 with permission from Elsevier.[150] Copyright 2020.

the solvent evaporation temperature and the atmosphere solvent saturation.[151] Methods such as flash infrared annealing and photonic curing are also R2R compatible.[152,153]

In the TSSP, both precursors are deposited separately. The BX_3 precursors are typically deposited first. The AX precursor is dissolved in a different solvent that would remove the BX_3 solvent, thus acting as an antisolvent. In both cases, the substrates are thermally annealed to remove any solvent traces and to promote grain growth.

The OSSP and TSSP each have their advantages and disadvantages. The OSSP is more straightforward since mixing all the precursors allows for an easier deposition, and it has a defined stoichiometry. However, the choice of antisolvent and how it is deposited greatly affects perovskite formation,[154] and the OSSP tends to result in big crystals with many pinholes, without homogeneous surface coverage.[150,155] Lead halide deposition in the TSSP is easier to control and more homogeneous, but there is little control over the resulting perovskite stoichiometry.[155] There are arguments in favor of both methods for high-volume production: the OSSP allows for the precise control of precursor compositions, enables the use of complicated perovskite formulations in high-efficiency devices, and has a more economic implementation.[156] TSSP allows for more consistent film morphology, leading to reproducible devices.[157] Regardless of which process is used, more than one solvent is required, often with distinct properties, and their interactions with the cellulose substrate need to be carefully considered.

Changing the solvents. Lead-based PSCs are generally prepared using a mixture of DMF and DMSO. DMF has been labeled as a solvent with "major issues" because of its high toxicity, which complicates PSC upscaling.[158] Moreover, it can redisperse certain types of cellulose (see Table S1), making it important to find a replacement.

Substituting DMF : DMSO with ethanol and acetonitrile. Ethanol and acetonitrile are incapable of dissolving lead iodide (PbI_2) on their own and are commonly used as cosolvents. Ethanol can be mixed with *N*,*N*-dimethylacetamide (DMA) and alkylammonium chloride (RNH_3Cl) to form $FAPbI_3$;[159] it is worth noting that DMA is a toxic solvent, but it is used in small amounts. In a similar fashion, acetonitrile can be mixed with 1,2-dimethoxyethane (DME) to make $FAPbI_3$[160] or with isopropyl acetate (IA) to make $MAPbI_3$.[161]

The use of a mixture of ethanol and acetonitrile was a significant advancement in PSC fabrication in recent years. In their work, Rezaee *et al.* fabricated $MAPbI_3$ PSCs on glass/ITO and PET/ITO *via* bar coating and slot-die coating, respectively, at room temperature and attained efficiencies of 19.5%.[162] A similar solvent mixture, DMSO with acetonitrile and ethanol, was used in the production of a wide-bandgap perovskite on tandem modules. The PSCs reached efficiencies up to 21.5%, and 23.8% in 20 cm^2 tandem devices.[163]

Substituting DMF : DMSO with water and IPA. Water is one of the main factors contributing to PSC degradation due to the critical role played by moisture in perovskite decomposition. This has led to researchers regarding water as unsuitable for PSC manufacturing. However, water and other green options can replace DMF and DMSO, the most commonly used solvents in lead-based PSC production. In the TSSP, BX_2 precursors are deposited first, followed by AX. PbI_2 has poor solubility in water, so it is replaced by $Pb(NO_3)_2$. Once dry, the substrate is submerged in a methylammonium iodide bath in IPA and thermally annealed to form the perovskite layer (Fig. 9).

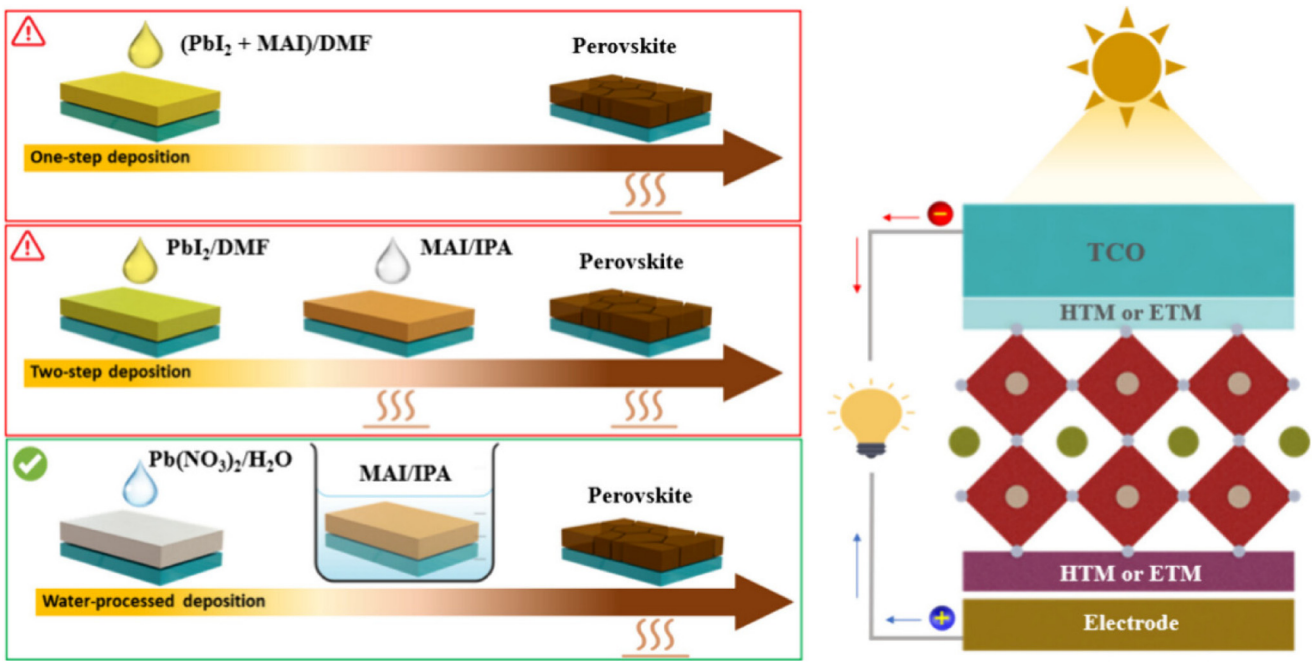

Fig. 9 PSC fabrication using water as a solvent, reproduced from ref. 167 with permission from the American Chemical Society.[167] Copyright 2024.

The crystallization pathway of perovskites formed from aqueous precursors differs from that of conventional organic-solvent systems, often producing films with larger grains.[164–166] Interestingly, studies showed water-processed PSCs exhibit enhanced stability compared with DMF-based devices due to the absence of excess PbI_2, the presence of larger crystalline domains, and $Pb(NO_3)_2$-derived residues that can act as water scavengers. Despite these advantages, some challenges still remain for aqueous precursor processing, including incomplete surface coverage, pinhole formation driven by Ostwald ripening, and the need for multi-cycle deposition to achieve uniform films. Surfactants such as potassium oleate have been introduced to lower the surface tension of water and promote better wetting. Using this strategy, PSCs have achieved 24% PCE, with unencapsulated devices retaining 92.5% of their initial performance after 90 days at 25 °C and 30% RH in ambient air. Under combined thermal and light stress (1 sun, 60 °C), these devices maintain 90.8% of their original PCE after 800 h, illustrating that properly controlled aqueous processing can deliver both high efficiency and long-term operational stability.

Moreover, while improved morphology, fewer defects, and controlled crystallization pathways explain much of the enhanced stability, broader degradation pathways, such as ion migration remain considerations.

Changing the antisolvent. An antisolvent is used to remove the perovskite solvent and induce crystallization. It needs to weakly interact with the perovskite precursors and simultaneously be miscible in the host solvent. Applying the antisolvent on the deposited perovskite films greatly reduces the solubility of the precursors and triggers fast nucleation, thus facilitating perovskite film formation. The antisolvent application time plays a pivotal role in the quality of the perovskite layer. Whether the application time is short or long depends on the miscibility of the antisolvent in the host solvent and on the solubility of the organic halides in the antisolvent. Taylor *et al.* demonstrated that high-performance devices can be made with a variety of antisolvents; the key lies in adjusting the application time (Fig. 10).[154] Based on this understanding, PSCs made on cellulose can be adapted to an antisolvent that is compatible with the substrate, which can lead to the use of green, nontoxic antisolvents.[168]

Solvent toxicity and environmental impact assessment. In comparison with lead, the toxicity of the solvents used in the processing of active and charge transport layers in PSCs is a less frequently discussed concern. The toxicity and environmental impacts of the solvents are just as important considerations, particularly as solution-based manufacturing approaches move toward industrialization. To quantitatively

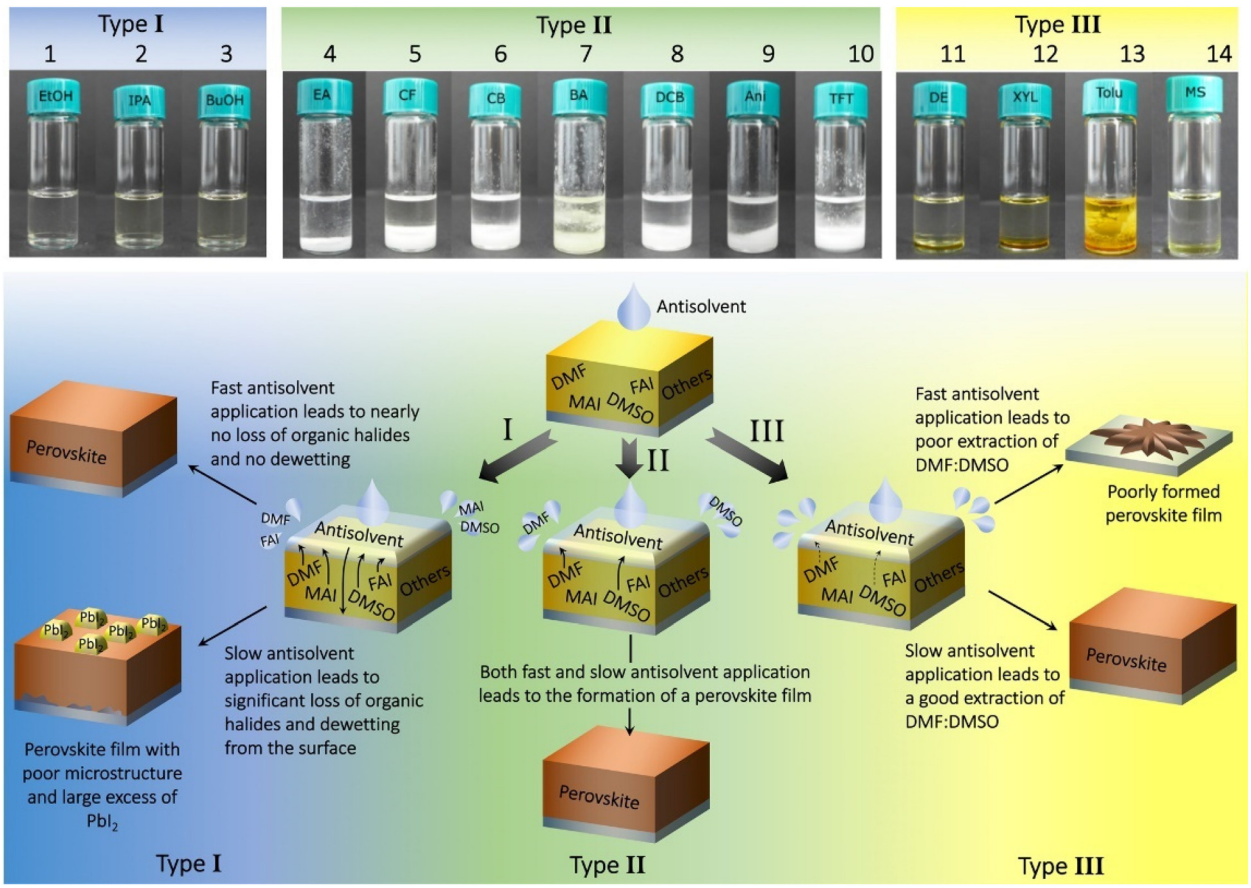

Fig. 10 Antisolvent application time chart, reproduced from ref. 154 with permission from Springer Nature.[154] Copyright 2021.

evaluate environmental and health impacts, Vidal *et al.*[169] conducted a full life-cycle assessment (LCA) covering industrial production, use, energy demand, emissions, and end-of-life handling for commonly used perovskite processing solvents. The findings showed that solvents such as DMF contribute disproportionately to human-health toxicity and environmental burdens. DMSO, which has a comparatively lower toxicity, is widely used as an additive in perovskite precursor solutions because its high donor number leads to the formation of stable intermediate phases.[170] Moreover, DMSO, although not acutely toxic, can cause dermal penetration of contaminants, creating additional safety concerns during large-scale perovskite coating.[170,171]

Using less toxic and more environmentally responsible solvent systems is essential for enabling safe and sustainable manufacturing. Green solvents, defined as low-toxicity, biodegradable, non-flammable with minimal environmental persistence, offer safer alternatives. Simple alcohols such as ethanol and IPA, water, and bio-derived solvents (*e.g.*, GVL) exhibit lower toxicity, biodegradability, and minimal bioaccumulation potential.[170] In addition, bio-derived solvents produced from renewable feedstocks offer further reductions in life-cycle impacts and align well with circular-economy principles. Taken together, both toxicity data and life-cycle assessment findings underscore that replacing hazardous polar aprotic solvents with greener alternatives can significantly reduce the environmental footprint associated with perovskite film fabrication. Table 10 presents the list of solvents used in the fabrication of PSCs classified based on Safety (S), Health (H), and Environment (E).

Step 9: thermal annealing

After the solvent is removed, the perovskite is annealed to promote crystal growth and remove any leftover solvent. This process is usually done at 100 °C for 40–60 minutes. As discussed earlier, high temperatures can cause cellulose to lose moisture and buckle, and additives like plasticizers to degrade, so it is prudent to minimize thermal treatments. The following methods can be used to anneal the perovskite layer at room temperature.

Gas quenching. If evaporation of the perovskite solvent can be modified, nitrogen gas can be used to quench the perovskite layer and effectively eliminate the need for an antisolvent (Fig. 11). In their study, Cassella *et al.* developed a perovskite ink with a 1 : 9 ratio of 2-methoxy ethanol and tetrahydrofuran (THF) and used it to make $MAPbI_3$ perovskite devices with up to 18% efficiency, without using an antisolvent or thermal annealing. The key finding was that THF helped accelerate the solvent removal by lowering the vapor pressure of the solvent mixture, facilitating the crystallization of the perovskite with just a nitrogen gas flow.[146] Caution is advised as both of these solvents are toxic. A similar approach could be found using non-toxic and greener solvents instead.

Water vapor annealing. An interesting technique for perovskite annealing at room temperature involves the use of water

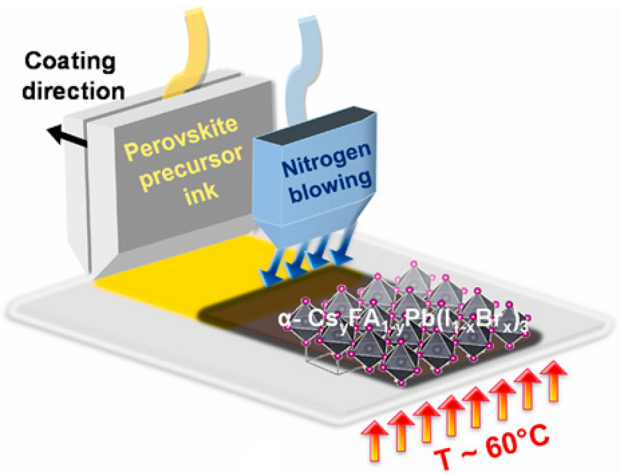

Fig. 11 Nitrogen gas quenching in slot-die process, adapted from ref. 151 with permission from Elsevier.[151] Copyright 2021.

Table 10 Safety, health, and environment scores for selected solvents scores are based on the CHEM21 solvent guide; higher numbers indicate worse scores. Adapted from ref. 172 with permission from the Royal Society of Chemistry.[172] Copyright 2016

Solvent	Role in PSC fabrication	Safety score	Health score	Environment score	Outcome
Water	Cleaning solvent media for SnO_2 and PEDOT, lead nitrate solvent	1	1	1	Recommended
Ethanol	Media for TiO_2, perovskite co-solvent and antisolvent	4	3	3	Recommended
IPA	Cleaning solvent, organic salt solvent	4	3	3	Recommended
Acetone	Cleaning solvent	5	3	5	Recommended
Methanol	MeO-2PACz solvent	4	7	5	Problematic
GVL	Perovskite solvent	1	5	7	Problematic
DMSO	Perovskite co-solvent	1	1	5	Problematic
DMF	Perovskite solvent	3	9	5	Hazardous
Chloroform	P3HT solvent	2	7	5	Highly hazardous
Chlorobenzene	SAMs, Spiro-OMeTAD, P3HT, and PTAA solvent, perovskite antisolvent	3	2	7	Problematic
Xylenes	Spiro-OMeTAD solvent	4	2	5	Problematic
Ethyl acetate	Spiro-OMeTAD solvent	5	3	3	Recommended
Toluene	PTAA solvent, perovskite antisolvent	5	6	3	Problematic
Diethyl ether	Perovskite antisolvent	10	3	7	Highly hazardous
Acetonitrile	Spiro-OMeTAD additives solvent, perovskite co-solvent	4	3	3	Problematic

vapor. The antisolvent is pipetted, and the substrates with the perovskite layer are kept under a moisture-controlled atmosphere for 60 minutes, during which the perovskite redissolves and recrystallizes as water evaporates. This approach has many advantages: it can be performed outside a glovebox and at room temperature; it produces low-hysteresis devices; and the resulting PSCs are more stable in moist environments than thermally annealed ones. Cells fabricated using this approach with simple $MAPbI_3$ perovskite achieved 16.4% efficiency.[173]

Ultrasonic vibration. Ultrasonic vibrations can be used to anneal the perovskite layer without thermal treatment (Fig. 12). After quenching the perovskite layer with antisolvent, vibrations are used to mix the perovskite components. This increases the solvent and antisolvent evaporation rates and the overall uniformity of the layer, which, in turn, contributes to efficiency, improved reproducibility, and reduced hysteresis.[174] Ultrasonic vibrations can even be used to make annealing-free and antisolvent-free perovskite layers, although the performance is quite low at 10.43% on mesoporous devices.[175] This technique has previously been used to anneal an SnO_2 CTL and a perovskite layer, resulting in an astonishing PCE level of 17.38% on flexible PET/ITO, entirely at room temperature.[130]

Doping. Dong *et al.* reported making $MAPbI_3$ PSCs with 19.25% efficiency entirely at room temperature. First, an SnO_2 ETL was deposited and cured with UV light, without any thermal annealing. Second, a perovskite precursor solution was doped with 0.1 mol ml^{-1} of guanidinium iodide, and the active layer underwent crystallization within a nitrogen-filled glovebox in one hour.[176] This work evidences the possibility of making high-efficiency PSCs at low temperatures.

Another way to avoid the thermal annealing of perovskite is by doping the antisolvent with 3,4-ethoxylenedioxythiophene (EDOT). The dopant fills any halide vacancies and thus helps passivate any defects in the perovskite layer, and it increases cell stability by reducing halide ion migration. This technique also slightly increases the open-circuit voltage and device stability in ambient air. Cells made with this approach have attained 20.12% PCE on glass/FTO and 15.58% on unspecified flexible substrates.[177]

Step 10: depositing the second CTL

With solution-based processes, special care needs to be taken to use a compatible solvent during the second CTL deposition to avoid affecting the perovskite active layer. Additionally, since the perovskite has already been deposited by this stage, the rest of the process needs to proceed at a low temperature.

In NIP devices, 2,2′,7,7′-tetrakis(*N*,*N*-di-p-methoxyphenylamine)9,9′-spirobifluorene (Spiro-OMeTAD) is the most popular material for HTLs. Initially used as an HTL in light-emitting diodes and dye-sensitized solar cells, Spiro-OMeTAD was adapted to PSCs due to its easy processability, good morphology, and ability to match the bands of perovskite types.[178] Its conductivity is much lower than that of most perovskites, so Spiro-OMeTAD needs to be doped; the most common dopants are 4-*tert*-butyl pyridine (*t*BP), LiTFSI, and FK209.[179] The biggest drawback of Spiro-OMeTAD is its low stability, arising from the dopants' interactions and degradations when in contact with perovskite, water, and oxygen.[178] Promising new HTL materials similar to Spiro-OMeTAD have been recently developed and have proved to be easier to synthesize and more stable.[180,181]

PTAA has also been used as an HTL in devices with the NIP structure. It requires doping with *t*BP and LiTFSI to become a p-type material, but the dopant concentration needed is four times less than that of Spiro-OMeTAD.[182] PTAA has many advantages: it is an amorphous, thermally stable material that is soluble in a wide range of organic solvents and forms very smooth films.[182,183] There is no clear winner between PTAA and Spiro-OMeTAD, as they both have advantages and disadvantages. PTAA is more mechanically and thermally stable, but Spiro-OMeTAD has been the preferred HTL material in record-breaking PSCs.[182]

Poly(3-hexylthiophene) (P3HT) is the third most commonly used organic material for the HTL in NIP PSCs. It exhibits good hole mobility without dopants and is inexpensive and simple to process. It is speculated to be a good replacement for Spiro-OMeTAD, as its low cost makes it a very attractive option for large-scale production.[184] P3HT devices have been reported to attain an impressive efficiency level of 24.6%.[185] The molecular structures of the different organic HTLs are illustrated in Fig. 13.

The deposition of metal oxide transport layers on the perovskite layer is uncommon because of the high temperatures necessary for deposition and annealing. One way to get around this issue is by synthesizing metal oxide NPs. NiO_x NPs printed in NIP devices and SnO_2 NPs in PIN devices have been reported to achieve 25.17% and 16.5% efficiency, respectively.[187,188]

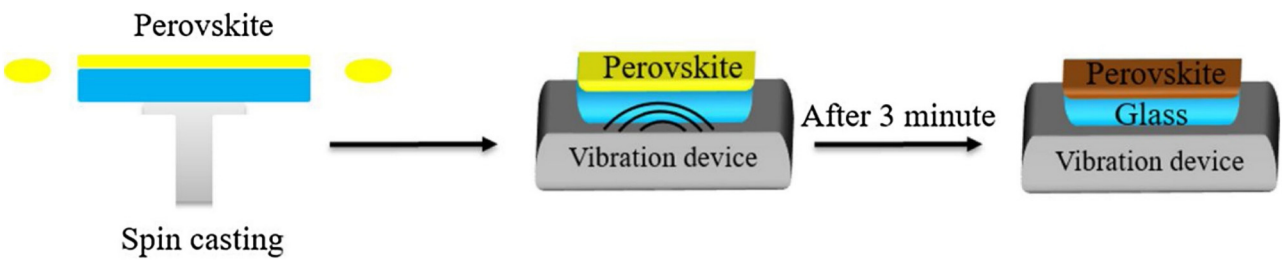

Fig. 12 Ultrasonic vibration annealing, reproduced from ref. 175 with permission from Elsevier.[175] Copyright 2018.

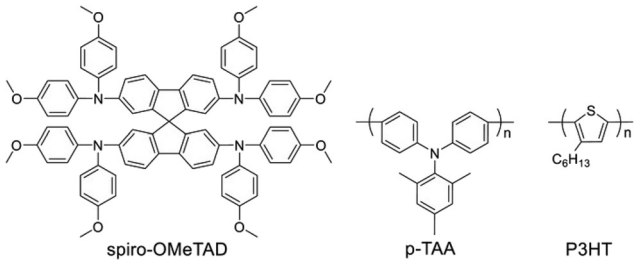

Fig. 13 Molecular structures of organic HTLs, adapted from ref. 186 with permission from Wiley.[186] Copyright 2021.

For PIN structure devices, fullerene and its derivatives (C60 and PCBM) are the most popular ETL choices, thanks to their low-temperature processing, high electron conductivity, and appropriate band alignment with perovskites. However, good quality C60 layers require thermal evaporation, whereas PCBM is processable in solution but dimerizes under light and absorbs the perovskite degradation products, thus losing stability.[189]

Changing the solvents

Substituting chlorobenzene with ethyl acetate. There is an urgent need to replace chlorobenzene (CB), a common antisolvent for lead-based PSCs and a common solvent for Spiro-OMeTAD, with an alternative, as it is highly toxic to animals and the environment, and large volumes are used during fabrication.[190] CB can be replaced with ethyl acetate (EA), a safer, greener alternative. Notably, devices made with Spiro-MeOTAD and EA have outperformed devices made with CB, at PCEs of 23.3% and 21.0%, respectively.[191] In a study that compared many solvents for Spiro-OMeTAD, it was proved that CB can be substituted with p-xylene, a less toxic and more industrially compatible solvent, and achieve an identical PCE.[192]

Step 11: top electrode

The last step in PSC fabrication is the deposition of the top electrode. Thermally evaporated metals such as gold, silver, aluminum, and copper are the most typical materials for this layer. Their main advantages are their high conductivity, ease of processability, and proper work function. Their biggest drawback is metal ion diffusion into the other layers, which lowers device stability.[193]

AgNWs can be used as top electrodes, and when combined with a TCO as a bottom electrode, they enable the easy fabrication of bifacial PSCs.[194] When an opaque substrate is used, such as titanium foil, the top electrode needs to be transparent to let light into the active layer.

Carbon is among the newest electrode materials proposed for PSCs. Carbon electrodes are normally used in mesoporous recyclable devices but have been adapted to work as top electrodes in planar devices. A composite carbon electrode can be hot pressed on top of Spiro-OMeTAD or P3HT (Fig. 14). Devices made with this novel technique have achieved efficiency levels of over 19%.[195] A similar approach has been taken in an R2R process involving a silver-carbon composite, which proves the scalability of this material.[196]

Outlook

Actionable points

Crosslinking is a key factor. Cellulose is usually dispersed in common solvents; this is useful since it allows for easy and safe processing, although it also means it can redisperse when coating it with materials dissolved in those solvents. As outlined in Steps 1 and 2, crosslinking cellulose can improve the films' solvent resistance,[12,31] and slightly decrease their CTE and gas permeation.[55,76] Crosslinking seems to be mostly done on hydrogels and membranes,[197,198] and rarely done on transparent films; it has the potential to make cellulose a viable alternative to PET and PEN as exemplified by cellulose vitrimers.[12]

New plasticizers. A certain level of flexibility is required to undertake the PSC production process, especially in R2R. Plasticization is an easy way to improve cellulose films' mechanical properties,[63,65] and even decrease gas permeation, with simple molecules such as sorbitol and maltitol.[65,66] One of cellulose's advantages over synthetic polymers is their relatively high temperature resistance. The issue with plasticiza-

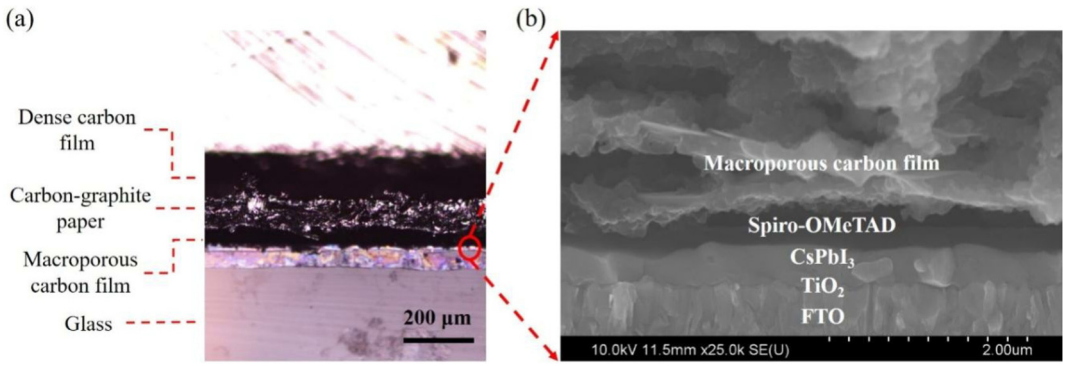

Fig. 14 Cross-section of hot-pressed composite carbon electrode over a PSC: (a) optical microscope image, (b) SEM image, reproduced from ref. 195 with permission from Springer Nature.[195] Copyright 2025.

tion is the degradation of the plasticizers at temperatures around 100 °C,[46] therefore, there is a need to find new plasticizing materials that can resist higher temperatures to ease manufacturing.

Decrease gas permeation. While crosslinking and plasticizers can increase the gas barrier properties of cellulose films, it still requires coatings to reach appropriate levels for optoelectronics.[93–95] Some ceramic coatings have been explored but require complicated techniques such as atomic layer deposition; if possible, more sustainable and easier methods should be explored.

Standardized CTE measurements. So far, CTE values for different types of cellulose have been reported, yet these studies use different instruments and testing conditions. Moreover, to our knowledge, there is no work that analyses the effects water loss and plasticizer degradation have on cellulose films CTE. This literature gap could be covered with a study that analyses CTE values of different types of cellulose films under the same measurement conditions.

Lead leakage and immobilization. Lead leakage in PSCs is a big concern that hinders their adoption.[199] Replacing the glass substrate with cellulose risks increasing the chance of lead leaking out of the devices, yet the substrate is not entirely responsible for this. Together with the encapsulant and immobilization methods, proper antileakage measures can be achieved without solely depending on the substrate. Moreover, coatings used to decrease gas permeation could also help to prevent lead leakages, although this has not been studied yet. Bio-based and organic materials show promising encapsulation[200–202] and lead immobilization[203,204] that can support cellulose substrates without diminishing the device's overall sustainability.

Reporting cellulose data that serves optoelectronics. Researchers have proposed cellulose as a potential substrate, but the available data are insufficient to convince the perovskite community to adopt it. Cellulose researchers need to offer data on the mechanical properties of their films, solvent vulnerabilities, OTR and WVTR values, their surface roughness, optical transmittance and haze, CTE values and temperature limits, and how all these properties compare to PEN and PET. Additionally, the data should be in the units normally used by the optoelectronics field. Providing these data would significantly help the optoelectronics field to adopt more sustainable substrate materials.

Economic and life-cycle assessments. There are some examples of PSCs built on cellulose substrates, although their efficiency is quite low compared to the state-of-the-art.[36,205,206] Once the fabrication process on cellulose has been optimized and their efficiency rivals that of PSCs built on PET and PEN, their costs and sustainability need to be quantified. Adapting technoeconomic[207,208] and life-cycle assessments[209,210] of PSCs on PET and PEN would be good starting points to show the benefits and future challenges of using bio-based substrates.

Maintaining sustainability in mind. The goal is to have solar cells that abide by circular economics. Using expensive or scarce materials and wasteful fabrication techniques undermines the purpose of substituting the substrate. Efforts to improve the properties of cellulose must be guided by a strong commitment to sustainability.

Summary

Over the last decade, PSCs have been considered promising options for circumventing the costly and energy-intensive fabrication of silicon. PSCs have undergone huge leaps in efficiency and stability, and now, before they enter the market, the question of their sustainability is taking center stage. Science and industry are increasingly aiming to integrate PSCs into a circular economy model, and cellulose might be one of the key factors. However, combining cellulose and PSCs comes with many intricacies that have rarely been explored; it is not as easy as merely swapping one material for another. A successful outcome requires both the cellulose and the PSC fields to come together and understand the other's needs and limitations, including acceptable gas barrier levels, appropriate transparency and conductivity values, and the solvent resistance of cellulose films, among others.

Cellulose has the potential to be a sustainable substrate but only after careful modifications and optimization. What would PSC fabrication on cellulose look like? First, cellulose needs to be crosslinked to increase its solvent resistance and reduce its CTE and water uptake. Next, plasticizers and other compounds have to be included to increase the flexibility of cellulose films, and coatings are needed to reduce gas permeation. Cellulose needs to be dried properly during casting for maximum transparency and minimum surface roughness. The most critical point arises during the deposition of the bottom electrode and the first CTL, as these have the biggest impacts on the deposition of the next layers and the overall quality of the device. Solvent compatibility and an appropriate surface morphology are crucial parameters at this stage. Finally, cleaning treatments, ink deposition, and annealing treatments need to be adapted to PSC processing to avoid damaging the substrate.

The traditional PSC processing route has to evolve to accommodate more sustainable approaches. Here, we offer some realistic solutions for most of the steps involved, which can be implemented with varying levels of engineering and optimization. The most challenging aspect is ensuring that the gas barrier properties of cellulose, particularly the oxygen barrier, surpass those of PET and PEN; OTR and WVTR levels need to improve to ensure that solar cells are both sustainable and long lasting. Otherwise, this technology would only be suitable for applications with short lifespans, such as some sensors and indoor photovoltaics. Gas barriers can be improved by pairing cellulose-based PSCs with biobased encapsulants, which would ensure the recyclability of the devices. Environmental, social, and economic sustainability and the high-throughput production of PSCs is within reach, and the methods have been laid out in this article. We hope that the outlined recommendations help perovskite and cell-

ulose experts come together in bringing forth the next generation of solar technology.

Author contributions

J. V. G.: conceptualization, investigation, visualization, methodology, writing – original draft, writing – review and editing, project administration; M. H.: writing – original draft, writing – review and editing; V. A.: investigation, writing – original draft; S. Y.: investigation; J. K.: writing – review and editing; R. S.: writing – review and editing; M. V.: writing – review and editing; K. M.: conceptualization, supervision, funding acquisition, writing – review and editing.

Conflicts of interest

There are no conflicts of interest to declare.

Data availability

The data supporting this article has been included as part of the supplementary information (SI). Supplementary information: Solvent resistance test film preparation and Table S1. Supplementary information is available. See DOI: https://doi.org/10.1039/d5gc05281e.

Acknowledgements

J. V. G. thanks the Research Council of Finland, project ECOSOL (347275). M. H. thanks PROFI7/SUSMAT funding provided by the Research Council of Finland. V. A., S. Y. and K. M. thank Circular Materials Bioeconomy Network funded by the Ministry of Education and Culture, Finland (CIMANET, Decision No. VN/3137/2024-OKM-6). J. K. acknowledges that she is part of the Sector Plan Engineering II, which is funded by the Dutch Ministry of Education, Culture, and Science (OCW). M. V. and R. S. acknowledge the support provided by the Research Council of Finland (RCF), Printed intelligence infrastructure funding, decision 358621 and the RCF Flagship Programme, Photonics Research and Innovation (PREIN), decision number 346545. The authors thank Väinö Anttalainen/University of Turku for photographing our cellulose solvent resistance experiment samples.

References

1 C. Yang, W. Hu, J. Liu, C. Han, Q. Gao, A. Mei, Y. Zhou, F. Guo and H. Han, *Light: Sci. Appl.*, 2024, **13**, 227.
2 R. G. Charles, A. Doolin, R. García-Rodríguez, K. V. Villalobos and M. L. Davies, *Energy Environ. Sci.*, 2023, **16**, 3711–3733.
3 E. S. Akulenko, M. Hadadian, A. Santasalo-Aarnio and K. Miettunen, *Heliyon*, 2023, **9**, e13584.
4 S. Kim, H. Van Quy and C. W. Bark, *Mater. Today Energy*, 2021, **19**, 100583.
5 P. Subudhi and D. Punetha, *Prog. Photovoltaics*, 2023, **31**, 753–789.
6 Y. Ma, Z. Lu, X. Su, G. Zou and Q. Zhao, *Adv. Energy Sustainability Res.*, 2022, **4**, DOI: 10.1002/aesr.202200133.
7 M. Tao, V. Fthenakis, B. Ebin, B. Steenari, E. Butler, P. Sinha, R. Corkish, K. Wambach and E. S. Simon, *Prog. Photovoltaics*, 2020, **28**, 1077–1088.
8 D. Le Khac, S. Chowdhury, A. Soheil Najm, M. Luengchavanon, A. Mebdir Holi, M. Shah Jamal, C. Hua Chia, K. Techato and V. Selvanathan, *Sol. Energy*, 2024, **267**, 112214.
9 G. S. Han, S. Lee, M. L. Duff, F. Qin and J.-K. Lee, *ACS Appl. Mater. Interfaces*, 2018, **10**, 4697–4704.
10 B. T. Feleki, R. K. M. Bouwer, M. M. Wienk and R. A. J. Janssen, *Sol. RRL*, 2022, **6**, 2100898.
11 J. Liu, T. Ye, D. Yu, S. (Frank) Liu and D. Yang, *Angew. Chem., Int. Ed.*, 2023, **62**, DOI: 10.1002/anie.202307225.
12 L. Huang, Y. Li, Z. Zheng, Y. Bai, T. P. Russell and C. He, *Mater. Horiz.*, 2024, **11**, 1560–1566.
13 B. Liu, J. Zeng, P. Li, M. Kui, J. Li and K. Chen, *Chem. Eng. J.*, 2024, **498**, 155273.
14 L. Gao, L. Chao, M. Hou, J. Liang, Y. Chen, H.-D. Yu and W. Huang, *npj Flexible Electron.*, 2019, **3**, 4.
15 G. Dinesh and B. Kandasubramanian, *Mater. Chem. Phys.*, 2022, **281**, 125707.
16 H. Qi, *Novel Functional Materials Based on Cellulose*, Springer International Publishing, 2017.
17 B. Lindman, G. Karlström and L. Stigsson, *J. Mol. Liq.*, 2010, **156**, 76–81.
18 H. Qi, *Novel Functional Materials Based on Cellulose*, Springer International Publishing, Cham, 2017.
19 N. B. Erdal and M. Hakkarainen, *Biomacromolecules*, 2022, **23**, 2713–2729.
20 S. Jing, L. Wu, A. P. Siciliano, C. Chen, T. Li and L. Hu, *ACS Nano*, 2023, **17**, 22196–22226.
21 O. A. El Seoud, M. Kostag, K. Jedvert and N. I. Malek, *Macromol. Mater. Eng.*, 2020, **305**, DOI: 10.1002/mame.201900832.
22 A. Forte, F. Dourado, A. Mota, B. Neto, M. Gama and E. C. Ferreira, *Int. J. Life Cycle Assess.*, 2021, **26**, 864–878.
23 A. Mazega, A. F. Lehrhofer, R. J. Aguado, A. Potthast, R. Marquez, T. Rosenau and M. Delgado-Aguilar, *Cellulose*, 2025, **32**, 5227–5246.
24 A. Babaei-Ghazvini, B. Vafakish, R. Patel, K. J. Falua, M. J. Dunlop and B. Acharya, *Int. J. Biol. Macromol.*, 2024, **258**, 128834.
25 T. Heinze, O. A. El Seoud and A. Koschella, in *Cellulose Derivatives*, Springer Cham, 1st edn, 2018, pp. 259–292.
26 T. Nishino, I. Matsuda and K. Hirao, *Macromolecules*, 2004, **37**, 7683–7687.
27 J. A. Diaz, X. Wu, A. Martini, J. P. Youngblood and R. J. Moon, *Biomacromolecules*, 2013, **14**, 2900–2908.

28 T. Zhang, P. Yang, M. Chen, K. Yang, Y. Cao, X. Li, M. Tang, W. Chen and X. Zhou, *ACS Appl. Mater. Interfaces*, 2019, **11**, 36010–36019.
29 W. A. MacDonald, *J. Mater. Chem.*, 2004, **14**, 4.
30 B. Xiong, W. Zhong, Q. Zhu, K. Liu, M. Li, G. Sun and D. Wang, *Nanoscale*, 2017, **9**, 19216–19226.
31 Z. Xiao, J. Liu, X. Chen, Z. Suo, X. Cao, N. Xu, Z. Yao, C. Li, X. Wan and Y. Chen, *J. Mater. Chem. A*, 2025, **13**, 2301–2308.
32 Š. Jech, N. Bartie, G. Tas, K. Miettunen, R. Serna-Guerrero and A. Santasalo-Aarnio, *Sol. Energy Mater. Sol. Cells*, 2025, **286**, 113561.
33 V. Larini, C. Ding, F. Faini, G. Pica, G. Bruni, L. Pancini, S. Cavalli, M. Manzi, M. Degani, R. Pallotta, M. De Bastiani, C. Ma and G. Grancini, *Adv. Funct. Mater.*, 2023, **34**, DOI: 10.1002/adfm.202306040.
34 G. Imbuluzqueta, F. J. Cano, U. Iglesias, J. Aizpurua, J. M. Hernández, N. Yurrita, W. Cambarau and O. Zubillaga, *Sol. Energy*, 2025, **300**, 113799.
35 G. Fredi and A. Dorigato, *Adv. Ind. Eng. Polym. Res.*, 2021, **4**, 159–177.
36 H. Li, X. Li, W. Wang, J. Huang, J. Li, Y. Lu, J. Chang, J. Fang and W. Song, *Sol. RRL*, 2019, **3**, DOI: 10.1002/solr.201800317.
37 X. Dai, Y. Deng, C. H. Van Brackle, S. Chen, P. N. Rudd, X. Xiao, Y. Lin, B. Chen and J. Huang, *Adv. Energy Mater.*, 2019, **10**, DOI: 10.1002/aenm.201903108.
38 J. H. Heo, D. H. Shin, M. L. Lee, M. G. Kang and S. H. Im, *ACS Appl. Mater. Interfaces*, 2018, **10**, 31413–31421.
39 C. Zhou, Y. Xu, Y. Li, K. Du, X. Li, X. Dong, L. Li, N. Yuan and J. Ding, *Sol. RRL*, 2023, **8**, DOI: 10.1002/solr.202300901.
40 N. Ren, L. Tan, M. Li, J. Zhou, Y. Ye, B. Jiao, L. Ding and C. Yi, *iEnergy*, 2024, **3**, 39–45.
41 X. Chen, W. Cai, T. Niu, H. Wang, C. Liu, Z. Zhang, Y. Du, S. Wang, Y. Cao, P. Liu, W. Huang, C. Ma, B. Yang, S. (Frank) Liu and K. Zhao, *Energy Environ. Sci.*, 2024, **17**, 6256–6267.
42 R. Xu, F. Pan, J. Chen, J. Li, Y. Yang, Y. Sun, X. Zhu, P. Li, X. Cao, J. Xi, J. Xu, F. Yuan, J. Dai, C. Zuo, L. Ding, H. Dong, A. K.-Y. Jen and Z. Wu, *Adv. Mater.*, 2023, **36**, DOI: 10.1002/adma.202308039.
43 A. Miglani, S. B. Ogale and O. S. Game, *Small*, 2025, **21**, DOI: 10.1002/smll.202411355.
44 J. Valdez García, M. Hadadian, R. Nizamov, P. Mäkinen, N. Lamminen, P. Vivo and K. Miettunen, *R. Soc. Open Sci.*, 2024, **11**, DOI: 10.1098/rsos.241012.
45 M. Saliba, J.-P. Correa-Baena, C. M. Wolff, M. Stolterfoht, N. Phung, S. Albrecht, D. Neher and A. Abate, *Chem. Mater.*, 2018, **30**, 4193–4201.
46 J. J. Benitez, P. Florido-Moreno, J. M. Porras-Vázquez, G. Tedeschi, A. Athanassiou, J. A. Heredia-Guerrero and S. Guzman-Puyol, *Int. J. Biol. Macromol.*, 2024, **273**, 132956.
47 Q. Wu, Y. Meng, K. Concha, S. Wang, Y. Li, L. Ma and S. Fu, *Ind. Crops Prod.*, 2013, **48**, 28–35.
48 Z. Wang, M. Zhu, J. Li, C. Hu, J. Li, R. Xiong and C. Huang, *Nano Energy*, 2024, **129**, 109974.
49 H. Yang, J. Edberg, V. Gueskine, M. Vagin, M. G. Say, J. Erlandsson, L. Wågberg, I. Engquist and M. Berggren, *Carbohydr. Polym.*, 2022, **278**, 118938.
50 G. Hu, X. Lan, B. Peng, J. Liao and Y. Xiong, *Int. J. Biol. Macromol.*, 2024, **260**, 129476.
51 Q. Yu, L. Yang, S. Wang, L. Zhang and D. Sun, *Cellulose*, 2023, **30**, 10273–10284.
52 W. Ge, J. Shuai, Y. Wang, Y. Zhou and X. Wang, *Polym. Chem.*, 2022, **13**, 359–372.
53 M. Nogi and H. Yano, *Appl. Phys. Lett.*, 2009, **94**, DOI: 10.1063/1.3154547.
54 A. A. Goje, N. A. Ludin, P. N. A. Fahsyar, U. Syafiq, P. Chelvanathan, A. D. A.-G. Syakirin, M. A. Teridi, M. A. Ibrahim, M. S. Su'ait, S. Sepeai and A. S. H. M. Yasir, *Mater. Renew. Sustain. Energy*, 2024, **13**, 155–179.
55 B. Guo, W. Chen and L. Yan, *ACS Sustainable Chem. Eng.*, 2013, **1**, 1474–1479.
56 T. H. Yim, S. H. Koo and H. Lee, *Curr. Appl. Phys.*, 2010, **10**, S241–S243.
57 L. Chen, H. Yu, M. Dirican, D. Fang, Y. Tian, C. Yan, J. Xie, D. Jia, H. Liu, J. Wang, F. Tang, X. Zhang and J. Tao, *Adv. Mater. Interfaces*, 2020, **7**, DOI: 10.1002/admi.202000928.
58 X. Sun, Q. Wu, X. Zhang, S. Ren, T. Lei, W. Li, G. Xu and Q. Zhang, *Cellulose*, 2018, **25**, 1103–1115.
59 M. Nogi, S. Iwamoto, A. N. Nakagaito and H. Yano, *Adv. Mater.*, 2009, **21**, 1595–1598.
60 Y. Wang, K. Li, X. Li, H. Cui, G. Liu, H. Xu, X. Wu, W. Yao, B. Zhong, X. Huang, H. Wang and T. Wu, *Carbon*, 2019, **152**, 873–881.
61 A. B. Catel, F. F. Camilo and C. Molina, *Opt. Mater.*, 2025, **165**, 117092.
62 A. Bouftou, K. Aghmih, F. Lakhdar, N. Abidi, S. Gmouh and S. Majid, *Measurement: Food*, 2024, **15**, 100180.
63 S. Paudel, S. Regmi and S. Janaswamy, *Food Packag. Shelf Life*, 2023, **37**, 101090.
64 E. Csiszár and S. Nagy, *Carbohydr. Polym.*, 2017, **174**, 740–749.
65 P. Ahokas, V. Kunnari, J. Majoinen, A. Harlin and M. Mäkelä, *ACS Sustainable Chem. Eng.*, 2025, **13**, 10771–10779.
66 N. Nasiri, H. E. Cainglet, G. Garnier and W. Batchelor, *Cellulose*, 2024, **31**, 7421–7436.
67 S. C. Teixeira, R. R. A. Silva, T. V. de Oliveira, P. C. Stringheta, M. R. M. R. Pinto and N. de F. F. Soares, *Food Biosci.*, 2021, **42**, 101202.
68 S. Guzman-Puyol, J. Hierrezuelo, J. J. Benítez, G. Tedeschi, J. M. Porras-Vázquez, A. Heredia, A. Athanassiou, D. Romero and J. A. Heredia-Guerrero, *Int. J. Biol. Macromol.*, 2022, **209**, 1985–1994.
69 J. Fernández-Santos, C. Valls, O. Cusola and M. B. Roncero, *Int. J. Biol. Macromol.*, 2022, **211**, 218–229.
70 K. Chi and J. M. Catchmark, *Food Hydrocolloids*, 2018, **80**, 195–205.

71 B. Fathi Achachlouei and Y. Zahedi, *Carbohydr. Polym.*, 2018, **199**, 415–425.
72 J. Valdez García, A. Boding, X. Yang, R. Nizamov, M. S. Reid, K. Junel, K. Miettunen, T. Abitbol and J. Kaschuk, *Int. J. Biol. Macromol.*, 2025, **292**, 139203.
73 S. Castro-Hermosa, M. Top, J. Dagar, J. Fahlteich and T. M. Brown, *Adv. Electron. Mater.*, 2019, **5**, DOI: 10.1002/aelm.201800978.
74 Nippon Electric Glass, Ultra-thin glass: G-Leaf, https://www.neg.co.jp/en/products/g-leaf/index.html, (accessed 17 September 2025).
75 Q.-H. Lu and F. Zheng, in *Advanced Polyimide Materials*, Elsevier, 2018, pp. 195–255.
76 T. J. Hickman, L. Tao, N. Stingelin and J. C. Meredith, *RSC Sustainability*, 2024, **2**, 3451–3455.
77 C. Sun, G. Li, J. Wang, Z. Fang, F. Qin, K. Chen, J. Zhou and X. Qiu, *Cellulose*, 2022, **29**, 7111–7124.
78 J. J. Kaschuk, Y. Al Haj, J. Valdez García, A. Kamppinen, O. J. Rojas, T. Abitbol, K. Miettunen and J. Vapaavuori, *Carbohydr. Polym.*, 2024, **332**, 121877.
79 A. W. Cindradewi, R. Bandi, C.-W. Park, J.-S. Park, E.-A. Lee, J.-K. Kim, G.-J. Kwon, S.-Y. Han and S.-H. Lee, *Polymers*, 2021, **13**, 2990.
80 M. N. Mirvakili, S. G. Hatzikiriakos and P. Englezos, *Phys. Fluids*, 2021, **33**, DOI: 10.1063/5.0043881.
81 I. Hasan, J. Wang and M. Tajvidi, *Cellulose*, 2021, **28**, 11345–11366.
82 G. Horvat, K. Žvab, Ž. Knez and Z. Novak, *Polymers*, 2022, **14**, 2399.
83 A. Kramar, I. Rodríguez Ortega, G. González-Gaitano and J. González-Benito, *Cellulose*, 2023, **30**, 2037–2052.
84 K. Shanmugam, H. Nadeem, C. Browne, G. Garnier and W. Batchelor, *Colloids Surf., A*, 2020, **589**, 124396.
85 F. Karasu, L. Müller, H. Ridaoui, M. Ibn ElHaj, G. Flodberg, C. Aulin, L. Axrup and Y. Leterrier, *Front. Chem.*, 2018, **6**, DOI: 10.3389/fchem.2018.00571.
86 P. Holzhey, M. Prettl, S. Collavini, C. Mortan and M. Saliba, *Sci. Rep.*, 2023, **13**, 6375.
87 M. Fahland, O. Zywitzki, T. Modes, K. Vondkar, T. Werner, C. Ottermann, M. Berendt and G. Pollack, *Thin Solid Films*, 2019, **669**, 56–59.
88 H. E. Lee, Y. Ji, Y. D. Kim, K. Kim and H. O. Seo, *Mater. Res. Bull.*, 2025, **185**, 113321.
89 S. Lee, S.-W. Lee, S. Bae, J.-K. Hwang, W. Lee, D. Pyun, S.-H. Jeong, K. Kim, J.-S. Hwang, S. Cho, D. Kim, Y. Kang and H.-S. Lee, *Energies*, 2023, **16**, 8061.
90 M. Socol, N. Preda, A. Costas, G. Petre, A. Stanculescu, I. Stavarache, G. Popescu-Pelin, S. Iftimie, A. Stochioiu, A. M. Catargiu and G. Socol, *Appl. Phys. A*, 2025, **131**, 17.
91 G. Zhang, H. Wu, C. Chen, T. Wang, J. Yue and C. Liu, *Nanoscale Res. Lett.*, 2015, **10**, 76.
92 Z. Guo, X. Li, N. Li, X. Liu, L. Hao, Y. Wang, W. Deng, H. Bai, J. Liang and Z. Chen, *Phys. Chem. Chem. Phys.*, 2024, **26**, 4524–4532.
93 J. J. Kaschuk, M. Borghei, K. Solin, A. Tripathi, A. Khakalo, F. A. S. Leite, A. Branco, M. C. Amores de Sousa, E. Frollini and O. J. Rojas, *ACS Appl. Polym. Mater.*, 2021, **3**, 2393–2401.
94 M. N. Mirvakili, H. Van Bui, J. R. van Ommen, S. G. Hatzikiriakos and P. Englezos, *ACS Appl. Mater. Interfaces*, 2016, **8**, 13590–13600.
95 S. Yue, S. Wang, D. Han, S. Huang, M. Xiao and Y. Meng, *Cellulose*, 2022, **29**, 8293–8303.
96 M. Fazeli, M. Keley and E. Biazar, *Int. J. Biol. Macromol.*, 2018, **116**, 272–280.
97 R. Yewale, P. Damlin, M. Salomäki and C. Kvarnström, *Mater. Today Commun.*, 2020, **25**, 101398.
98 X. Hu, X. Meng, L. Zhang, Y. Zhang, Z. Cai, Z. Huang, M. Su, Y. Wang, M. Li, F. Li, X. Yao, F. Wang, W. Ma, Y. Chen and Y. Song, *Joule*, 2019, **3**, 2205–2218.
99 P. Kumar, W.-J. Lee, Y. Tang, H. Yang, W. Xu, P. Rout, L. You, J. A. Romo, B. Pradhan, J. Mei and L. Dou, *EES Sol.*, 2025, **1**, 529.
100 Y. Ding, S. Xiong, L. Sun, Y. Wang, Y. Zhou, Y. Li, J. Peng, K. Fukuda, T. Someya, R. Liu and X. Zhang, *Chem. Soc. Rev.*, 2024, **53**, 7784–7827.
101 J. Sun, X. Li, Z. Chen, S. Yan, L. Qin, J. Zeng, S. Wang, J. Xu, L. Zhao, W. Zhou, Q. Wang, H. Gong, A. Lu and J. Yu, *Org. Electron.*, 2018, **63**, 392–397.
102 R. J. B. Pinto, M. A. Martins, J. M. F. Lucas, C. Vilela, A. J. M. Sales, L. C. Costa, P. A. A. P. Marques and C. S. R. Freire, *ACS Appl. Mater. Interfaces*, 2020, **12**, 34208–34216.
103 J. Kim, W. J. da Silva, A. R. bin Mohd Yusoff and J. Jang, *Sci. Rep.*, 2016, **6**, 19813.
104 M. Lagrange, D. P. Langley, G. Giusti, C. Jiménez, Y. Bréchet and D. Bellet, *Nanoscale*, 2015, **7**, 17410–17423.
105 S. Han, S. Hong, J. Ham, J. Yeo, J. Lee, B. Kang, P. Lee, J. Kwon, S. S. Lee, M. Yang and S. H. Ko, *Adv. Mater.*, 2014, **26**, 5808–5814.
106 J. Gong, X. Fan, Z. Zong, M. Yang, Y. Sun and G. Zhao, *RSC Adv.*, 2023, **13**, 15531–15539.
107 S. J. Lee, Y.-H. Kim, J. K. Kim, H. Baik, J. H. Park, J. Lee, J. Nam, J. H. Park, T.-W. Lee, G.-R. Yi and J. H. Cho, *Nanoscale*, 2014, **6**, 11828–11834.
108 M. Betker, C. Harder, E. Erbes, J. E. Heger, A. E. Alexakis, B. Sochor, Q. Chen, M. Schwartzkopf, V. Körstgens, P. Müller-Buschbaum, K. Schneider, S. A. Techert, L. D. Söderberg and S. V. Roth, *ACS Appl. Nano Mater.*, 2023, **6**, 13677–13688.
109 D. Li, L. Wang, W. Ji, H. Wang, X. Yue, Q. Sun, L. Li, C. Zhang, J. Liu, G. Lu, H.-D. Yu and W. Huang, *ACS Appl. Mater. Interfaces*, 2021, **13**, 1735–1742.
110 B. Kang and F. Yan, *Energy Environ. Sci.*, 2025, **18**, 3917–3954.
111 X. Wang, H. Jin, R. C. R. Nagiri, B. Z. L. Poliquit, J. Subbiah, D. J. Jones, N. Kopidakis, P. L. Burn and J. Yu, *Sol. RRL*, 2019, **3**, DOI: 10.1002/solr.201800286.
112 J. Linnemann, J. Giorgio, K. Wagner, G. Mathieson, G. G. Wallace and D. L. Officer, *J. Mater. Chem. A*, 2015, **3**, 3266–3270.
113 Y. Galagan, D. J. D. Moet, D. C. Hermes, P. W. M. Blom and R. Andriessen, *Org. Electron.*, 2012, **13**, 3310–3314.

114 H. Li, X. Li, W. Wang, J. Huang, J. Li, S. Huang, B. Fan, J. Fang and W. Song, *Sol. Energy*, 2019, **188**, 158–163.
115 F. C. Krebs, T. Tromholt and M. Jørgensen, *Nanoscale*, 2010, **2**, 873.
116 N. Espinosa, R. García-Valverde, A. Urbina and F. C. Krebs, *Sol. Energy Mater. Sol. Cells*, 2011, **95**, 1293–1302.
117 M. Österberg, M. S. Peresin, L.-S. Johansson and T. Tammelin, *Cellulose*, 2013, **20**, 983–990.
118 M. Zuber, K. M. Zia, I. A. Bhatti, Z. Ali, M. U. Arshad and M. J. Saif, *Int. J. Biol. Macromol.*, 2012, **51**, 743–748.
119 C. Wang, Z. Yuan, A. Wang, J. Qu, Z. Fang and Y. Wen, *Cellulose*, 2020, **27**, 2041–2051.
120 R. A. Wolf, *Atmospheric pressure plasma for surface modification*, John Wiley & Sons, Hoboken, N.J, 1st edn, 2013.
121 J. L. Carter, C. A. Kelly and M. J. Jenkins, *Polym. J.*, 2023, **55**, 253–260.
122 D. Shin, D. Kang, J.-B. Lee, J.-H. Ahn, I.-W. Cho, M.-Y. Ryu, S. W. Cho, N. E. Jung, H. Lee and Y. Yi, *ACS Appl. Mater. Interfaces*, 2019, **11**, 17028–17034.
123 S. Y. Lee, G. Y. Park, N. Kim, M. Kang, K. Kim, S. Cho, W. Choi, J. S. Myung and D. S. Ham, *Energy Technol.*, 2023, **12**, DOI: 10.1002/ente.202301058.
124 Z. Xu, X. Zhou, X. Li and P. Zhang, *Sol. RRL*, 2022, **6**, DOI: 10.1002/solr.202200092.
125 A. Kojima, K. Teshima, Y. Shirai and T. Miyasaka, *J. Am. Chem. Soc.*, 2009, **131**, 6050–6051.
126 F. Gayot, E. Bruhat, M. Bouttemy, M. Frégnaux, E. De Vito, J.-P. Kleider, S. Cros and M. Manceau, *ACS Appl. Energy Mater.*, 2023, **6**, 11849–11860.
127 A. A. Eliwi, M. Malekshahi Byranvand, P. Fassl, M. R. Khan, I. M. Hossain, M. Frericks, S. Ternes, T. Abzieher, J. A. Schwenzer, T. Mayer, J. P. Hofmann, B. S. Richards, U. Lemmer, M. Saliba and U. W. Paetzold, *Mater. Adv.*, 2022, **3**, 456–466.
128 Z. Li, Z. Wang, C. Jia, Z. Wan, C. Zhi, C. Li, M. Zhang, C. Zhang and Z. Li, *Nano Energy*, 2022, **94**, 106919.
129 S. Y. Park and K. Zhu, *Adv. Mater.*, 2022, **34**, DOI: 10.1002/adma.202110438.
130 X. Zhang, F. Zabihi, H. Xiong, M. Eslamian, C. Hou, M. Zhu, H. Wang and Q. Zhang, *Chem. Eng. J.*, 2020, **394**, 124887.
131 J. Wang, Z. Dong, J. Wang, J. Zhang, Z. Zhai, F. Qiu, J. Wu, Y. Lin and J. Zhang, *J. Mater. Chem. A*, 2023, **11**, 22206–22215.
132 S. Li, X. Wang, N. Huang, S. He, L. Qiu and Y. Qi, *EnergyChem*, 2024, **6**, 100135.
133 A. Kabdiyeva, A. Zeinidenov, D. Abeuov, X. Rozhkova and A. Aimukhanov, *Opt. Mater.*, 2026, **169**, 117581.
134 L. Zhou, Y. Du, J. Zhang, X. Feng, D. Chen, W. Zhu, H. Xi, J. Zhang, C. Zhang and Y. Hao, *Chem. Eng. J.*, 2025, **511**, 161813.
135 S. Liu, J. Li, W. Xiao, R. Chen, Z. Sun, Y. Zhang, X. Lei, S. Hu, M. Kober-Czerny, J. Wang, F. Ren, Q. Zhou, H. Raza, Y. Gao, Y. Ji, S. Li, H. Li, L. Qiu, W. Huang, Y. Zhao, B. Xu, Z. Liu, H. J. Snaith, N.-G. Park and W. Chen, *Nature*, 2024, **632**, 536–542.
136 Y. Zheng, T. Niu, L. Chao, Y. Xia and Y. Chen, *J. Energy Chem.*, 2025, **107**, 74–86.
137 J. J. Lee, S. Gandla, B. Lim, S. Kang, S. Kim, S. Lee and S. Kim, *NPG Asia Mater.*, 2020, **12**, 65.
138 X. Dong, X. Zhou, Y. Liu, S. Xiong, J. Cheng, Y. Jiang and Y. Zhou, *Energy Environ. Sci.*, 2023, **16**, 1511–1519.
139 Y. Yoo, G. Seo, H. J. Park, J. Kim, J. Jang, W. Cho, J. H. Kim, J. Shin, J. S. Choi, D. Lee, S.-W. Baek, S. Lee, S. M. Kang, M. Kim, Y.-E. Sung and S. Bae, *J. Mater. Chem. A*, 2024, **12**, 1562–1572.
140 G. C. Wilkes, X. Deng, J. J. Choi and M. C. Gupta, *ACS Appl. Mater. Interfaces*, 2018, **10**, 41312–41317.
141 A. H. Ghahremani, B. Martin, A. Gupta, J. Bahadur, K. Ankireddy and T. Druffel, *Mater. Des.*, 2020, **185**, 108237.
142 P. Wang, X. Zhang, Z. Zhang, H. Ling, L. Tao, K. Sohail, X. Li, X. Fu, X. Zhang, R. Wang, Y. Wang, J. Luo, M. J. Ko, J. Chen and Y. Li, *ACS Appl. Energy Mater.*, 2023, **6**, 6554–6562.
143 Z. Xu, L. Huang, Y. Jiang, Z. Li, C. Chen, Z. He, J. Liu, Y. Fang, K. Wang, G. Zhou, J.-M. Liu and J. Gao, *ACS Appl. Mater. Interfaces*, 2022, **14**, 41037–41044.
144 P.-H. Lee, T.-T. Wu, C.-F. Li, D. Głowienka, Y.-H. Sun, Y.-T. Lin, H.-W. Yen, C.-G. Huang, Y. Galagan, Y.-C. Huang and W.-F. Su, *Chem. Eng. J.*, 2021, **412**, 128746.
145 Y. Wang, Q. Chen, J. Fu, Z. Liu, Z. Sun, S. Zhang, Y. Zhu, X. Jia, J. Zhang, N. Yuan, Y. Zhou, B. Song and Y. Li, *Chem. Eng. J.*, 2022, **433**, 133265.
146 E. J. Cassella, E. L. K. Spooner, J. A. Smith, T. Thornber, M. E. O'Kane, R. D. J. Oliver, T. E. Catley, S. Choudhary, C. J. Wood, D. B. Hammond, H. J. Snaith and D. G. Lidzey, *Adv. Energy Mater.*, 2023, **13**, DOI: 10.1002/aenm.202203468.
147 F. U. Kosasih, E. Erdenebileg, N. Mathews, S. G. Mhaisalkar and A. Bruno, *Joule*, 2022, **6**, 2692–2734.
148 S.-R. Bae, D. Y. Heo and S. Y. Kim, *Mater. Today Adv.*, 2022, **14**, 100232.
149 S. Tao, I. Schmidt, G. Brocks, J. Jiang, I. Tranca, K. Meerholz and S. Olthof, *Nat. Commun.*, 2019, **10**, 2560.
150 S. Chaudhary, S. K. Gupta and C. M. Singh Negi, *Mater. Sci. Semicond. Process.*, 2020, **109**, 104916.
151 M. Fievez, P. J. Singh Rana, T. M. Koh, M. Manceau, J. H. Lew, N. F. Jamaludin, B. Ghosh, A. Bruno, S. Cros, S. Berson, S. G. Mhaisalkar and W. L. Leong, *Sol. Energy Mater. Sol. Cells*, 2021, **230**, 111189.
152 S. Sánchez and A. Hagfeldt, in *Perovskite Solar Cells*, Wiley, 2021, pp. 33–89.
153 M. A. Slimani, S. G. Cloutier and R. Izquierdo, *Nanomaterials*, 2024, **14**, 886.
154 A. D. Taylor, Q. Sun, K. P. Goetz, Q. An, T. Schramm, Y. Hofstetter, M. Litterst, F. Paulus and Y. Vaynzof, *Nat. Commun.*, 2021, **12**, 1878.
155 M. Li, Y.-M. Xie, X. Xu, Y. Huo, S.-W. Tsang, Q.-D. Yang and Y. Cheng, *Org. Electron.*, 2018, **63**, 159–165.

156 D. Angmo, G. DeLuca, A. D. Scully, A. S. R. Chesman, A. Seeber, C. Zuo, D. Vak, U. Bach and M. Gao, *Cell Rep. Phys. Sci.*, 2021, **2**, 100293.
157 P. Kumar, *Appl. Phys. A*, 2024, **130**, 566.
158 J. Han, R. H. Kim, S. Huang, J. Kim and J. S. Yun, *Sol. RRL*, 2024, **8**, DOI: 10.1002/solr.202400262.
159 H.-S. Yun, H. W. Kwon, M. J. Paik, S. Hong, J. Kim, E. Noh, J. Park, Y. Lee and S. Il Seok, *Nat. Energy*, 2022, **7**, 828–834.
160 X. Huang, F. Cao, S. Zhan, Q. Feng, M. Zhu, Z. Su, X. Gao, J. Yin, J. Li, N. Zheng and B. Wu, *Joule*, 2023, **7**, 1556–1573.
161 Y. Yang, Y. Wang, Z. Qu, K. Zhang, T. Liang, S. Chen, W. Lv, F. Min, Y. Chen, Y. Qiao and Y. Song, *Angew. Chem., Int. Ed.*, 2023, **62**, DOI: 10.1002/anie.202300971.
162 E. Rezaee, D. I. Kutsarov, J. Zhang, G. Koutsourakis, B. Li, F. A. Castro and S. R. P. Silva, *Small Methods*, DOI: 10.1002/smtd.202300564.
163 C. Duan, H. Gao, K. Xiao, V. Yeddu, B. Wang, R. Lin, H. Sun, P. Wu, Y. Ahmed, A. D. Bui, X. Zheng, Y. Wang, J. Wen, Y. Wang, W. Ou, C. Liu, Y. Zhang, H. Nguyen, H. Luo, L. Li, Y. Liu, X. Luo, M. I. Saidaminov and H. Tan, *Nat. Energy*, 2025, **10**, 318–328.
164 Y. Zhang, L. Ren, P. Zhai, J. Xin, J. Wu, Q. Zhang, X. Chen, K. Zhao, L. Zhang and S. (Frank) Liu, *Energy Environ. Sci.*, 2024, **17**, 296–306.
165 D. V. Shinde, L. Pyeon, M. Pei, G.-W. Kim, H. Yang and T. Park, *ACS Appl. Mater. Interfaces*, 2017, **9**, 14023–14030.
166 T. Hsieh, M. Pylnev, E. Palomares and T. Wei, *Adv. Funct. Mater.*, 2020, **30**, DOI: 10.1002/adfm.201909644.
167 M. T. Hoang, Y. Yang, N. D. Pham and H. Wang, *J. Phys. Chem. Lett.*, 2024, **15**, 6880–6889.
168 Y. Yang, Z. Huang, H. Gao, Z. Xu, W. Fang, Y. Chen, Y. Hu, Z. Yi, J. Huang and H. Zhu, *RSC Adv.*, 2024, **14**, 32370–32388.
169 R. Vidal, J.-A. Alberola-Borràs, S. N. Habisreutinger, J.-L. Gimeno-Molina, D. T. Moore, T. H. Schloemer, I. Mora-Seró, J. J. Berry and J. M. Luther, *Nat. Sustain.*, 2020, **4**, 277–285.
170 N.-G. Park, *Nat. Sustain.*, 2020, **4**, 192–193.
171 E. Greul, P. Docampo and T. Bein, *Z. Anorg. Allg. Chem.*, 2017, **643**, 1704–1711.
172 D. Prat, A. Wells, J. Hayler, H. Sneddon, C. R. McElroy, S. Abou-Shehada and P. J. Dunn, *Green Chem.*, 2016, **18**, 288–296.
173 B. Wang, Z.-G. Zhang, S. Ye, H. Rao, Z. Bian, C. Huang and Y. Li, *J. Mater. Chem. A*, 2016, **4**, 17267–17273.
174 H. Xiong, F. Zabihi, H. Wang, Q. Zhang and M. Eslamian, *Nanoscale*, 2018, **10**, 8526–8535.
175 M.-R. Ahmadian-Yazdi and M. Eslamian, *Mater. Today Commun.*, 2018, **14**, 151–159.
176 H. Dong, S. Pang, F. He, H. Yang, W. Zhu, D. Chen, H. Xi, J. Zhang, Y. Hao and C. Zhang, *Sol. RRL*, 2021, **5**, DOI: 10.1002/solr.202100097.
177 C. Dong, J. Chen, C.-H. Chen, Y.-R. Shi, W.-F. Yang, K.-L. Wang, Z.-K. Wang and L.-S. Liao, *Nano Energy*, 2022, **94**, 106866.
178 Y. Dong, F. M. Rombach, G. Min, H. J. Snaith, C.-T. Lin, S. A. Haque and T. J. Macdonald, *Mater. Sci. Eng., R*, 2025, **162**, 100875.
179 T. H. Schloemer, J. A. Christians, J. M. Luther and A. Sellinger, *Chem. Sci.*, 2019, **10**, 1904–1935.
180 S. Daskeviciute-Geguziene, A. Magomedov, M. Daskeviciene, K. Genevičius, N. Nekrašas, V. Jankauskas, K. Kantminiene, M. D. McGehee and V. Getautis, *Chem. Commun.*, 2022, **58**, 7495–7498.
181 S. Daskeviciute, Y. Zhang, M. Daskeviciene, K. Rakstys, J. Petrulevicius, V. Jankauskas, V. Getautis and M. K. Nazeeruddin, *Sol. RRL*, 2025, **9**, DOI: 10.1002/solr.202500034.
182 F. M. Rombach, S. A. Haque and T. J. Macdonald, *Energy Environ. Sci.*, 2021, **14**, 5161–5190.
183 Y. Ko, Y. Kim, C. Lee, Y. Kim and Y. Jun, *ACS Appl. Mater. Interfaces*, 2018, **10**, 11633–11641.
184 H. Kassem, A. Salehi and M. Kahrizi, *Energy Technol.*, 2024, **12**, DOI: 10.1002/ente.202301032.
185 M. J. Jeong, K. M. Yeom, S. J. Kim, E. H. Jung and J. H. Noh, *Energy Environ. Sci.*, 2021, **14**, 2419–2428.
186 Y. Zhang, Y. Ren, X. Xie, Y. Wei, L. He, L. Fang, J. Zhang, Y. Yuan and P. Wang, *Adv. Funct. Mater.*, 2021, **32**, DOI: 10.1002/adfm.202108855.
187 Y. Xu, Z. Chu, H. Wang, Z. Xing, B. Fan, X. Hu and Y. Chen, *Sci. China: Chem.*, 2024, **67**, 2335–2340.
188 S. Chapagain, B. Martin, P. Armstrong, C. L. Perkins, M. O. Reese, T. Druffel and C. A. Grapperhaus, *ACS Appl. Energy Mater.*, 2023, **6**, 4496–4502.
189 W. Zhang, X. Guo, Z. Cui, H. Yuan, Y. Li, W. Li, X. Li and J. Fang, *Adv. Mater.*, 2024, **36**, DOI: 10.1002/adma.202311025.
190 S. Hyun Park, I. Su Jin and J. Woong Jung, *Chem. Eng. J.*, 2021, **425**, 131475.
191 B. Guo, X. Chen, H. Luo, G. O. Odunmbaku, T. Jiang, N. A. N. Ouedraogo, Z. Huang, Q. Gao, B. Zhang, Y. Ouyang, Y. Pan, T. Xia, C. Wang, K. Zahid, C. Li, S. Chen, Y. Zheng, Z. Ma and K. Sun, *Sol. RRL*, 2023, **8**, DOI: 10.1002/solr.202300934.
192 F. Isabelli, F. Di Giacomo, H. Gorter, F. Brunetti, P. Groen, R. Andriessen and Y. Galagan, *ACS Appl. Energy Mater.*, 2018, **1**, 6056–6063.
193 A. Hassan, M. I. Syauqi, Y. Liu, Z. Ke, W. Lin, Z. Wang, Y. Jin and R. Azmi, *Mater. Sci. Eng., R*, 2025, **166**, 101023.
194 Q. Fu, J. He, J. Zheng, Y. Xing, Q. Wang, J. Xiong, W. Zhu, R. Xuan, A. Fu, X. Gan, L. Huang, X. Liu, Y. Zhu and J. Zhang, *J. Alloys Compd.*, 2024, **1001**, 175058.
195 B. Yu, J. Shi, Y. Li, S. Tan, Y. Cui, F. Meng, H. Wu, Y. Luo, D. Li and Q. Meng, *Nat. Commun.*, 2025, **16**, 3328.
196 L. J. Sutherland, D. Vak, M. Gao, T. A. N. Peiris, J. Jasieniak, G. P. Simon and H. Weerasinghe, *Adv. Energy Mater.*, 2022, **12**, DOI: 10.1002/aenm.202202142.

197 J. Batta-Mpouma, G. Kandhola, J. Sakon and J.-W. Kim, *Biomacromolecules*, 2022, **23**, 4085–4096.
198 C. Liu, X. Li, T. Liu, Z. Liu, N. Li, Y. Zhang, C. Xiao and X. Feng, *J. Membr. Sci.*, 2016, **512**, 1–12.
199 P. Wu, S. Wang, X. Li and F. Zhang, *Matter*, 2022, **5**, 1137–1161.
200 G. Zhang, Y. Zheng, H. Wang, G. Ding, F. Yang, Y. Xu, J. Yu and Y. Shao, *Joule*, 2024, **8**, 496–508.
201 R. N. Hussein and T. B. Carmichael, *ACS Appl. Electron. Mater.*, 2025, **7**, 9249–9266.
202 Y. Yang, J. Zhao, H. Yang, X. Yang, Y. Lu, Z. Huang, S. Duo, Z. Xiong and X. Hu, *Nat. Commun.*, 2025, **16**, 8993.
203 J. Li, X. Qiao, B. He, Y. Zhang, S. Pal, L. Sun, M. Bilal, Z. Su, X. Gao, J. Briscoe, I. Abrahams, M. Li, Z. Li and Y. Lu, *Energy Environ. Sci.*, 2025, **18**, 5632–5642.
204 Y. Xie, H. Sui, X. Chen, X. Wang, C. Li, H. Zhao, H. Zhong, C. Yao, S. Zhang and Q. Zhang, *Electrochim. Acta*, 2026, **545**, 147731.
205 S. Castro-Hermosa, J. Dagar, A. Marsella and T. M. Brown, *IEEE Electron Device Lett.*, 2017, **38**, 1278–1281.
206 L. Gao, L. Chao, M. Hou, J. Liang, Y. Chen, H.-D. Yu and W. Huang, *npj Flexible Electron.*, 2019, **3**, 4.
207 P. Holzhey, M. Prettl, S. Collavini, N. L. Chang and M. Saliba, *Joule*, 2023, **7**, 257–271.
208 L. McGovern, E. C. Garnett, S. Veenstra and B. van der Zwaan, *Sustainable Energy Fuels*, 2023, **7**, 5259–5270.
209 T. Okoroafor, A. Maalouf, S. Oez, V. Babu, B. Wilk and S. Resalati, *J. Cleaner Prod.*, 2022, **373**, 133665.
210 X. Tian, S. D. Stranks and F. You, *Nat. Sustain.*, 2021, **4**, 821–829.

